DEVELOPMENT OF MANGANESE-DOPED HYDROXYAPATITE INCORPORATED PCL ELECTROSPUN 3D SCAFFOLDS COATED WITH GELATIN FOR BONE TISSUE ENGINEERING

A THESIS SUBMITTED TO
THE GRADUATE SCHOOL OF NATURAL AND APPLIED SCIENCES
OF
MIDDLE EAST TECHNICAL UNIVERSITY

BY

ALALEH SAMIEI

IN PARTIAL FULFILLMENT OF THE REQUIREMENTS
FOR
THE DEGREE OF MASTER OF SCIENCE
IN
BIOMEDICAL ENGINEERING

JANUARY 2023

Approval of the thesis:

DEVELOPMENT OF MANGANESE-DOPED HYDROXYAPATITE INCORPORATED PCL ELECTROSPUN 3D SCAFFOLDS COATED WITH GELATIN FOR BONE TISSUE ENGINEERING

submitted by **ALALEH SAMIEI** in partial fulfillment of the requirements for the degree of **Master of Science** i**n Biomedical Engineering, Middle East Technical University** by,

Prof. Dr. Halil Kalıpçılar
Dean, Graduate School of **Natural and Applied Sciences** _____

Prof. Dr. Vilda Purutçuoğlu
Head of the Department, **Biomedical Engineering** _____

Prof. Dr. Dilek Keskin
Supervisor, **Biomedical Engineering, METU** _____

Prof. Dr. Zafer Evis
Co-Supervisor, **Engineering Sciences, METU** _____

Examining Committee Members:

Prof. Dr. Ayşen Tezcaner
Engineering Sciences, METU _____

Prof. Dr. Dilek Keskin
Engineering Sciences, METU _____

Prof. Dr. Caner Durucan
Metallurgical and Materials Eng., METU _____

Assist. Prof. Özge Erdemli
Molecular Biology and Genetics, Başkent University _____

Assist. Prof. Arda Büyüksungur
Basic Medical Sciences, Faculty of Dentistry, Ankara University _____

Date: 27.01.2023

I hereby declare that all information in this document has been obtained and presented in accordance with academic rules and ethical conduct. I also declare that, as required by these rules and conduct, I have fully cited and referenced all material and results that are not original to this work.

Name Last name : Alaleh Samiei

Signature :

ABSTRACT

DEVELOPMENT OF MANGANESE-DOPED HYDROXYAPATITE INCORPORATED PCL ELECTROSPUN 3D SCAFFOLDS COATED WITH GELATIN FOR BONE TISSUE ENGINEERING

Samiei, Alaleh
Master of Science, Biomedical Engineering
Supervisor : Prof. Dr. Dilek Keskin
Co-Supervisor: Prof. Dr. Zafer Evis

January 2023, 82 pages

Combination of polymers and bioceramics has increased their importance in bone tissue engineering (BTE) to treat various defects. Within this frame, in this thesis, it is aimed to develop a 3D gelatin-coated PCL scaffold combined with Mn-doped hydroxyapatite (HA) in order to investigate the effect of the doping element, i.e., the manganese (Mn) ion, on the structural and biological properties of the composite scaffold. Pure and Mn-doped HAs were synthesized using microwave irradiation, and the samples were sintered at 800, 900, and 1000°C. Following the evaluation of the microstructural and biological results, HA and Mn-doped HA samples sintered at 900°C were chosen for scaffold fabrications and analysis. PCL scaffold was initially constructed by electrospinning method, and gelatin-coating was done by the glutaraldehyde (GTA) cross-linker around the primary PCL scaffold. Final gelatin-coated PCL scaffold was synthesized at 10%, 15%, and 16% (w/v) PCL amounts. After the optimization, 15% (w/v) PCL coated with gelatin was modified further by adding HA and Mn-HA at two different concentrations (2.5 wt.% and 5 wt.%). Final PCL/gelatin/HA and PCL/gelatin/Mn-HA were characterized by in-vitro

degradation, bioactivity, and direct cytotoxicity tests. It was concluded that PCL/gelatin with 5mol% Mn-HA had better biological properties and characteristics for BTE applications.

Keywords: Bone Tissue Engineering, PCL/Gelatin scaffold, Manganese-doped Hydroxyapatite, Electrospinning, GTA Crosslinking

ÖZ

KEMİK DOKU MÜHENDİSLİĞİ İÇİN JELATİN KAPLI MANGANEZ KATKILI HİDROKSİAPATİT İÇEREN PCL ELEKTROEĞRİLMİŞ 3D İSKELELERİN GELİŞTİRİLMESİ

Samiei, Alaleh
Yüksek Lisans, Biyomedikal Mühendisliği
Tez Yöneticisi: Prof. Dr. Dilek Keskin
Ortak Tez Yöneticisi: Prof. Dr. Zafer Evis

Ocak 2023, 82 sayfa

Polimerlerin ve biyoseramiklerin kombinasyonu, çeşitli defektleri tedavi etmek için kemik doku mühendisliği (BTE) alanında önemini arttırmıştır. Bu kapsamda, bu çalışma, Mn-doped hidroksiapatit (HA) ile birlikte 3D jelatin kaplı PCL doku iskelesi geliştirmek amacıyla katkı elementi olan manganez (Mn) iyonunun kompozit iskelerin yapısal ve biyolojik özelliklerine etkisini araştırmak için tasarlanmıştır. Saf ve Mn-doped HA, mikrodalga ısıtması kullanılarak sentezlenmiş ve örnekler 800, 900 ve 1000°C'de sinterlenmiştir. Mikro yapısal ve biyolojik sonuçların değerlendirilmesinden sonra, HA ve Mn-doped HA örnekleri 900°C'de sinterlenmiş ve daha ileri iskele imalatı ve analiz için seçilmiştir. PCL iskele, ilk olarak elektroeğirme yöntemi ile inşa edilmiş ve jelatin PCL iskele etrafında glutaraldehit (GTA) çapraz-bağı kullanılarak jelatin kaplama yapılmıştır. Son jelatin kaplı PCL iskele, %10, %15 ve %16 (w/v) PCL konsantrasyonunda analiz edilmiştir. Optimizasyon sonrası, %15 (w/v) PCL, jelatin kaplamalı ve daha sonra HA ve Mn-HA ile iki farklı konsantrasyon (%2.5 wt.% ve %5 wt.%) eklenmiştir. Son PCL/jelatin/HA ve PCL/jelatin/Mn-HA, biyo-bozunum, biyouyumluluk ve direk

sitotoksisite testleri ile karakterize edilmiştir. PCL/jelatin ile 5mol% Mn-HA'nın BTE uygulamaları için daha iyi özelliklere sahip olduğu sonucuna varılmıştır.

Anahtar Kelimeler: Kemik Doku Mühendisliği, PCL/Jelatin İskele, Manganez-Katkılı Hidroksiapatit, Elektroeğirme, GTA Çapraz Bağlama

In memory of my dad for his love, guidance, and encouragement

ACKNOWLEDGMENTS

I would like to express my sincere gratitude to all the people who have supported me throughout my research.

First and foremost, I would like to thank my advisor Prof. Dilek Keskin and my co-advisor, Prof. Zafer Evis, for their unwavering support, guidance, and encouragement throughout the entire process. Their insights and expertise have been invaluable in helping me to shape and focus my research.

I would like to extend my thanks to all my friends and labmates for their help and support. I would like to thank Dr. Hossein Jodati who mentored me and whom I learned from a lot throughout my research and I'm very grateful for his help and support. I would like to thank my senior labmates Dr. Ahmet Engin Pazarçeviren, Dr. Mustafa Nakipoğlu, Idil Uysal, and Mustafa Bahadır Güner for teaching me so much during my study, and helping and supporting me throughout my research.

I would like to thank all my friends for their unconditional support. I would like to thank my labmate and friend Ataollah Nosratinia for being a good mentor from the beginning, and sharing his experience and knowledge to help me during my study. I would like to thank my friends Diner Tekeşanoska and Fatemeh Sarasir for being there for me anytime I need and for morally supporting me all the time.

I am also profoundly grateful to my family and friends for their love and support, which have been a constant source of strength throughout this endeavor.

Lastly, I would like to express my deep gratitude to my father, who passed away before I could share this accomplishment with him. His love and guidance have been with me every step of the way. He always encouraged me to achieve more academically and inspired me to be more ambitious and accomplish more.

TABLE OF CONTENTS

LIST OF TABLES

TABLES

LIST OF FIGURES

FIGURES

CHAPTER 1

INTRODUCTION

1.1 Tissue Engineering

The field of Tissue Engineering (TE) is described as an interdisciplinary field that combines the principles of biological sciences with engineering fields, in order to create and develop new biological substitutes to enhance, maintain, and repair the functionality of tissues. Since the goal of TE is to create functional tissues, understanding the concept of tissue formation and regeneration became an important part of this field (Lysaght & Reyes, 2001).

TE and regenerative medicine (RM) are two *in vitro* techniques that have emerged in response to the rising demand for donor tissues and organs. Limitations of organ and tissue transplantation, such as tissue rejection by the host, transportation issues, and the shortage of organ donors led to the emergence and development of TE and RM fields. These two fields combine the knowledge of different fields (i.e., biology, chemistry, medicine, engineering, pharmaceutical, and material sciences) in order to create novel treatments or materials for replacing damaged tissues and organs. TE can be used for both chronic and mild injuries; for example, patients with skin burns, bone defects, gastrointestinal tissue repair, etc. can benefit from the bioengineered and functional tissues that can be made by TE applications (Lanza et al, 2020).

Due to the effectiveness in fabricating nonwoven 3D structures, the electrospinning technique has gained a lot of interest. The electrospun structures such as scaffolds or membrane has a considerable degree of surface-to-volume ratio and it forms proper interconnected network-shaped nanofibrous structures; these features make the electrospun structures ideal for biomedical applications like TE, drug delivery

systems, etc. Additionally, various materials including synthetic polymers, natural polymers, or a combination of both, can be used in formation of nanofibrous scaffolds with the help of electrospinning method. Primarily, the scaffolds should contain the structural and functional properties of the natural ECM (extracellular matrix) which provides a suitable environment for cell activities and provides mechanical support. Thus, electrospun composite scaffolds can be a good option for bone healing and regeneration (Choi & Kim, 2012).

1.1.1 Bone Tissue Engineering

Over the past few decades, the field of bone tissue engineering has grown extensively due to the growing demand for bone repair applications across the world. In the US and other parts of the world, there is a significant growth in the demand for functional bone grafts. Each year, more than 500 thousand people in the United States receive treatments for bone defects at a cost of more than $2.5 billion (Amini et al., 2012).

There are a lot of limitations towards the autologous and allogenic transplantations due to the donor site morbidity, immune system rejection, pathogen transfer, and limited availability of donor tissue. Nevertheless, autografts and allografts are the most commonly used approaches for bone treatment. Autografts are generally used because of their histocompatibility and non-immunogenicity, and they contain bone morphogenic proteins (BMPs) and other growth factors needed for osteoinductivity. Allografts are the second most commonly used approach for bone repair. Similar to autografts, allografts are histocompatible, and they can be provided in a variety of forms, such as demineralized bone matrix (DBM), cortical grafts, osteochondral and whole-bone segments, etc. Both autografts and allografts have drawbacks, like donor site injury and morbidity, surgical risks, immunoreaction probabilities, and availability of donor site. Due to these factors, the field of bone tissue engineering has expanded in recent years (Amini et al., 2012; Ghasemi-Mobarakeh et al., 2019).

Bone tissue engineering (BTE) emerged three decades ago, and its goal is to create an alternative treatment that would overcome the drawbacks of conventional methods (autologous and allogenic transplantation). BTE approaches focus on main components, mainly: i) a scaffold that is biocompatible and can mimic the structure of the natural bone extra cellular matrix (ECM) besides having bioactive molecules that will enable osteoconduction with bone, ii) osteogenic cells or stem cells to be introduced in scaffolds, iii) specific signal molecules for cell differentiation, and adequate vascularization for supplying enough nutrients to the cells. Hence, the BTE field helps the regeneration of the bone tissue by substitution of a scaffold that resembles the natural bone structure (Figure 1.1) (Amini et al., 2012).

Many adult tissues contain stem cells and progenitors that can develop into new tissue with one or more connective tissue phenotypes; these cells are known as connective tissue progenitors. These progenitors require a suitable surface to adhere, proliferate and differentiate throughout the area where new tissue is needed. 3D porous scaffold is a proper surface that provides an environment for cell attachment and growth. The main concerns in the formation of scaffolds are the materials used, the 3D architecture of the scaffold, and the biochemical and mechanical properties of the scaffold's surface. Another important consideration for the scaffold's design and functionality is the characteristic behavior of the scaffold before and after its degradation (Muschler et al., 2004).

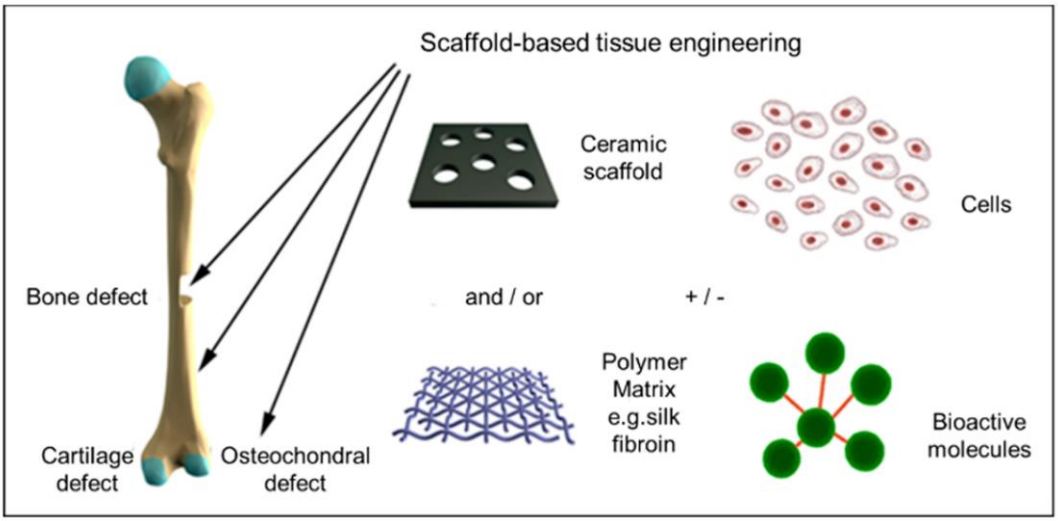

Figure 1.1 Bone regeneration through bone tissue engineering (Wu et al., 2020)

1.1.1.1 Bone Structure

Bone tissue has a composite structure that contains minerals, extracellular matrix, cells and water. It has a dynamic structure, and highly vascularized (Amini et al., 2012; Khurana et al., 2010); it continuously produces new tissues and remodels itself. During the growth phase, bone increases in size and shape which is called skeletal modeling. During late childhood and adulthood, bone has the ability to remodel itself which allows the skeleton to renew its tissue. Bone formation and resorption must be coupled to function simultaneously in order for skeletal modeling and remodeling to occur. Inorganic minerals, an organic matrix, cells, and water are the fundamental building blocks of the bone. The final structure of the bone is created by the hardening of the bone matrix and entrapment of osteoblasts (Breeland et al., 2022; Mohamed, 2008; Safadi et al., 2009).

Bone can be classified as inorganic (mineral) and organic, in terms of its microstructural organization. Sixty percent of the bone is mainly composed of hydroxyapatite (HA) whose stoichiometric formula is $Ca_{10}(PO_4)_6(OH)_2$. The organic

part is made up of osteoid, including collagen, and non-collagenous proteins which mainly contains glycoprotein, proteoglycan, phosphoproteins, and phospholipids (Figure 1.2) (Khurana et al., 2010).

Besides calcium and phosphate, which are the main components of bone mineral in the form of hydroxyapatite, other elements such as potassium, sodium, chloride, fluoride, etc. can be found in the inorganic portion of the bone. The common substitution is the carbonate which is placed for phosphate groups. The carbonate concentration is 4-6%, making the carbonated apatite. Additionally, other elements like magnesium, potassium, and sodium can be substituted in place of calcium ions, and elements such as fluoride and chloride can be substituted in place of hydroxyl ions. The substation of these elements, known as impurities can modify the crystallinity and solubility of mineral part of the bone (Feng, 2009; Morgan et al., 2013).

Type I collagen, which makes up 40% of the dry bone weight, is the main organic element of the bone matrix (Khurana et al., 2010). Collagen Type I is produced within the cells and by the formation of bonds between aligned triple helical collagen fibrils, the tropocollagen (collagen subunit) chains are formed (Figure 1.2) (Boraschi-Diaz et al., 2017; Wallace et al., 2011). Bone defects can be developed from the abnormalities in the structure of the bone; for instance, mutation in Type I collagen can lead to the loss of the normal organization of the bone's osteon (bone functional unit). Collagen has an important role in the regulation of the toughness, strength, and the flexibility of the bone. The mineral phase, which controls the stiffness of the bone, interacts with the collagen within the bone. The configuration of each collagen fibril affects the mechanical properties of the bone as well. That being the case, collagen is a promising biomaterial for use in different bone diseases due to its contribution in mechanical properties and its abundance within bone structure as the major component (Mallick et al., 2022; Petre & Leeuwenburgh, 2022)

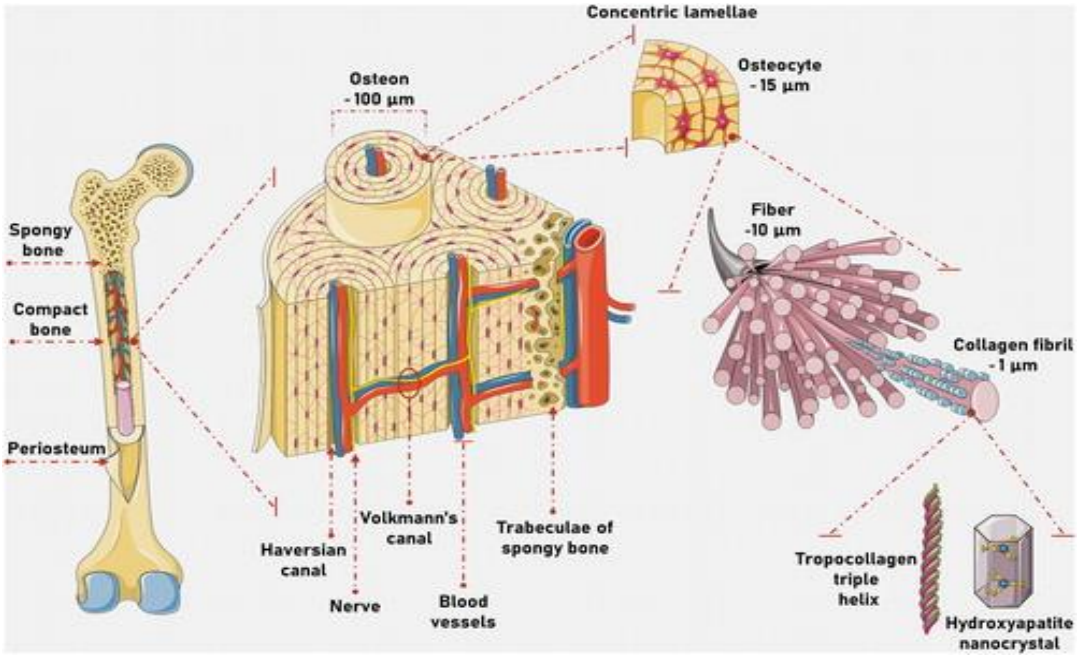

Figure 1.2. Structure of the bone (Petre & Leeuwenburgh, 2022)

Another classification of the bone is based on its shape; and it can be categorized as long, short, flat, irregular, and sesamoid bones (Figure 1.3) (Mallick et al., 2022; Mohamed, 2008).

All 4 types of bone mentioned above are structured with an outer cortical bone layer, also known as the cortex. The long bone is made up of a hollow shaft, also called the diaphysis, the cone-shaped metaphysis, and the rounded epiphyses below and above the growth plates, respectively. The metaphysis and epiphysis are composed of the trabecular (spongy) mesh-like structure which is covered by the cortical (dense, compact) bone layer. In contrast, the diaphysis is mainly made of dense cortical bone (Clarke, 2008).

The periosteum, perichondrium, and endosteum are tissue layers in and around the bone. The bone’s outer sheath, known as the periosteum, which is a fibrous connective tissue sheath, provides bone with blood, nerves, and the cells (osteoblasts and osteoclasts) for growth and healing. Sharpey's fibers, which are thick

collagenous fibers that extend into the underlying bone tissue, securely bind the periosteum to the outer cortical surface of the bone. The membrane that lines the inner surface of the cortical bone, trabecular bone, and the blood vessel canals, is covered by endosteum. The endosteum, which has blood vessels, osteoblasts, and osteoclasts, is in contact with the bone marrow space, trabecular bone, and blood vessel canals. Perichondrium and periosteum are relatively similar. Perichondrium covers the cartilage at the ends of the bone. The perichondrium has cells that stimulate the growth of new cartilage in required areas, similar to how the periosteum aids in the growth and healing of the bone (Clarke, 2008; Nahian & Chauhan, 2022).

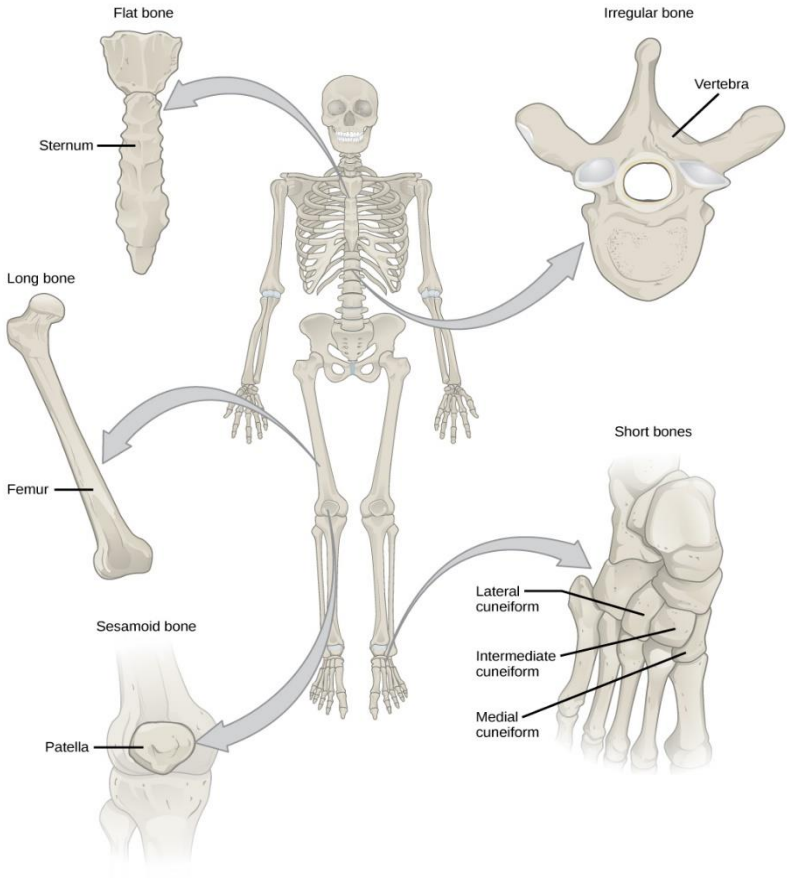

Figure 1.3. Classification of the bone according to its shape (Molnar & Gair, 2015)

1.1.1.2 Bone Matrix

Bone matrix is mainly composed of 40% organic phase (type I collagen) and 60% inorganic or mineral phase (calcium phosphate in the form of HA). Other than collagen type I, the organic part consists of proteoglycans, phospholipids, glycoproteins, phosphoproteins, and several collagenous and non-collagenous proteins such as osteocalcin, osteopontin, bone sialoprotein, and osteonectin. The inorganic part of the bone is comprised of crystalline HA in its calcium-deficient or carbonated form (Khurana et al., 2010; Mohamed, 2008).

The configuration of collagen with HA is in parallel form, which is created when HA crystals are stacked between the collagen gaps, called 'gap zones' or 'hole zone', in their parallel array. The collagen/HA arrangement gives rise to the composite structure of the bone. These structures containing parallel arrangements of mineralized collagen fibers form one lamella (3-7μm). The lamella is organized into concentric circles and forms a central canal that carries the blood vessels and nerve fibers inside the bone. This cylindrical structure with diameter of 200μm is called osteon or Haversian system. Based on previous studies, the collagen fibrils' orientation constantly changes from one lamella to the next, resulting in the twisted plywood structure. Osteons are aligned along stress line in compact bone, which helps the bone to resist bending or fracture (Molnar & Gair, 2015).

1.1.1.3 Bone Cells

Natural bone structure contains four different cell types: osteoblasts, osteoclasts, osteocytes and bone lining cells. Osteoblasts, osteoclasts, and bone lining cells are derived from progenitor cells which are also called mesenchymal stem cells, and they are present on the surface of the bone. When the bone is neither at the formation nor resorption stage, its surface is covered with bone-lining cells. It indicates that there's little sign of synthesis within these regions of the bone based on their organelle content, and they are called post proliferative osteoblasts. After covering

the surface of the bone, osteoclasts are unable to perform their resorption activity and therefore, there won't be any bone resorption or formation at these sites. Bone lining cells can later become reactivated to form osteoblasts (Clarke, 2008; Khurana et al., 2010; Mohamed, 2008).

Osteocytes are the post-proliferated and most mature (differentiated) form of osteoblasts. These cells are placed in lacunae, which are regularly distributed and lots of fine canals called canaliculi are radiated from them in all directions. Due to their vast distribution and interconnections, osteocytes are good candidates for stress detection within bone, and hence, they act as main mechanoreceptors of the bone. The structure of osteocytes may differ according to their position in relation to the bone surface. Some of the osteocytes have high activity and high organelle contents, similar to osteoblasts; other osteocytes are less active, and they are placed deeply with continuation of bone formation process (Clarke, 2008; Khurana et al., 2010; Mohamed, 2008).

Osteoblasts are bone forming cells; they are derived from osteoprogenitor cells which originated from pluripotent mesenchymal stem cells of the bone. Osteoblasts have cuboidal shape in their active form, and they are found on the surface of the bone during bone formation. The main function of osteoblasts is to synthesize the components of bone ECM (extra cellular matrix). They are also able to enhance bone mineralization by matrix vesicles in osteoid. Matrix vesicles possess alkaline phosphatase, adenosine triphosphatase (ATPases), and inorganic pyrophosphatase. These vesicles act as seeding sites for the formation of HA crystals by enzymatic accumulation of calcium and phosphate. The crystal growth initiates and proceeds from these sites which would gradually form apatite network. Collagen type I also can help mineralization by binding and orienting proteins like osteonectin which nucleates hydroxyapatite (Clarke, 2008; Khurana et al., 2010; Mohamed, 2008).

Osteoclasts are the cells that are responsible for bone resorption (degradation) in remodeling process and during pathologic state when bone resorption is increased (Figure 1.4). They are derived from osteoclast precursors (OCPs) which are

regulated by osteoblast during bone remodeling. Osteoclasts and osteoblasts together help degradation and formation of new bone tissue in natural remodeling process (Boyce et al., 2009).

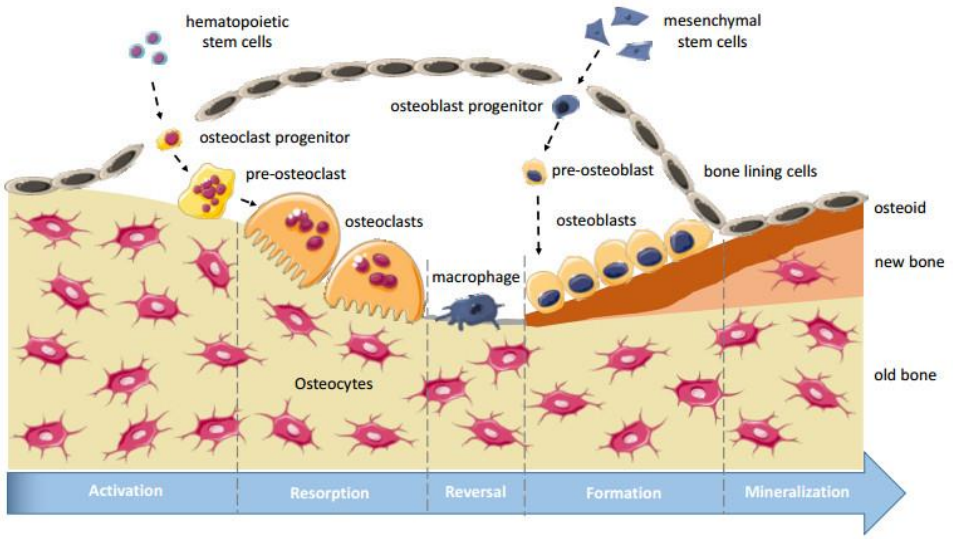

Figure 1.4. Bone cells and bone remodeling (Truesdell & Saunders, 2020)

1.2 Biomaterials

The field of biomaterials science has emerged by the combination of biological science and engineering fields, and it plays an important role in enhancement and treatment of incurable diseases. A nonviable material used in medical devices with the intent to interact with biological systems, was the first definition of the term “biomaterial” in 1987 (Williams, 1987). Along with the term “biomaterial”, another crucial concept called “Biocompatibility” was defined as the capacity of a material to function with an appropriate host response in a particular application (Ratner et al., 2013).

Since many applications, such as drug delivery and tissue engineering, contain living components (i.e., cells and other active agents), the term “nonviable” in the previous definition of “biomaterials” has lost its applicability. The following is the most recent definition of biomaterials that was agreed upon at the conference in 2018: a material intended to be designed in a specific way that can control the progress of a therapeutic or diagnostic operation through interactions with living systems (Ghasemi-Mobarakeh et al., 2019).

Biomaterials can be classified according to their origin as synthetic (i.e., metals, ceramics, polymers, and composites) and natural or biological (i.e., organic, and non-organic compounds derived from human, animals, or vegetable sources). Also, biomaterials can be classified as inert, bioactive, and bio-resorbable materials according to the host response (i.e., living tissues and organs) (Arjunan et al., 2021; Henao et al., 2019).

1.2.1 Bioceramics

Bioceramics can be defined as materials with ceramic origin; they can be used as metal coatings for biocompatibility improvement of the metallic material, they can be used as tissue replacements, or as a resorbable lattices in order to be used as short-term replacement of the tissue until the body creates new tissue.

Bioceramics have been significantly used to replace and restore hard tissues such as bone, tooth, and calcified cartilages at osteochondral interfaces, due to the similarities between physiochemical structure of the bioceramics and natural tissues (Jodati et al., 2020).

1.2.1.1 Hydroxyapatite

The stoichiometric formula of hydroxyapatite (HA) is $Ca_{10}(PO_4)_6(OH)_2$ that shows HA contains calcium and phosphate in its main structure. The stochiometric calcium

to phosphate ratio of HA is 1.67; any decrease from this value indicates the formation of calcium deficient or carbonated hydroxyapatite. The calcium-deficient form of HA is mainly resulted from the presence of various ions either within HA lattice structure or on the surface of the crystals. Both cationic and anionic substitution can occur within HA structure. Due to the presence of ions in natural bone structure, the ionic substitution has been considered in order to have more resemblance to the natural composition of the bone. The addition of different ions into HA lattice structure can affect the biological and physiochemical properties of the synthesized HA. The physiochemical properties are affected by the type of ionic substitution (cationic or anionic) on the Ca^{2+}, PO_4^{3-} and OH^- substitution sites. Also, ion substitution can modify crystallinity, crystalline phases, microstructure, thermal decomposition, solubility, and dissolution. Therefore, the contribution of the ions within bone structure can affect bone formation and prevention of bone diseases (Cacciotti, 2019; Jodati et al., 2020).

1.2.1.2 Ion-doped Hydroxyapatite

In order to mimic the structure of the bone in terms of chemical and biological compositions, different ions can be substituted (doped) within HA structure. These ions include magnesium (Mg), manganese (Mn), copper (Cu), selenium (Se), boron (B), etc. These ions can be added based on their effects on total HA structure; they can improve biocompatibility, mechanical, and other physiochemical properties (Yedekçi et al., 2022).

Two different crystal forms can exist for HA, the hexagonal and monoclinic forms; the hexagonal form has the lattice parameters of $a = b = 9.432$ Å, $c = 6.881$ Å, and $\gamma = 120°$, and monoclinic form has the lattice parameters of $a = 9.421$ Å, $b = 2a$, $c = 6.881$ Å, and $\gamma = 120°$. The characterization of these two forms is based on their Ca/P =1.67 ratio, and they are primarily different in the orientation of their hydroxyl group. Since hydroxyapatite has a high degree of structural flexibility, it can accommodate half of the elements in the periodic table into its sublattices, including

Ca^{2+}, OH, and PO_4^{3-}. Bivalent cations such as Sr^{2+}, Ba^{2+}, Mn^{2+}, Mg^{2+}, etc., and monovalent cations like Na^{+}, K^{+}, etc., can substitute Ca^{2+} in HA lattice structure. Moreover, the anionic substitution can occur in both OH and PO_4^{3-} positions. For instance, F^{-} and Cl^{-} can occupy OH^{-} site, and CO_3^{2-} element can substitute with OH^{-} and PO_4^{3-} (Figure 1.5). These ion substitutions can result in the formation of Ca-deficient or carbonated form of HA which is normally present in the natural bone structure (Cacciotti, 2019; Landi et al., 2003).

There are different methods that can be used to synthesize ion-doped HA; these methods include sol-gel, chemical precipitation, and hydrothermal methods. Recently, synthesis of HA was done using microwave-assisted irradiation and hydrothermal methods due the simplicity and rapid formation of HA powder. This method would give high crystallinity HA powders in short duration of time (Alshemary et al., 2018; Yedekçi et al., 2022).

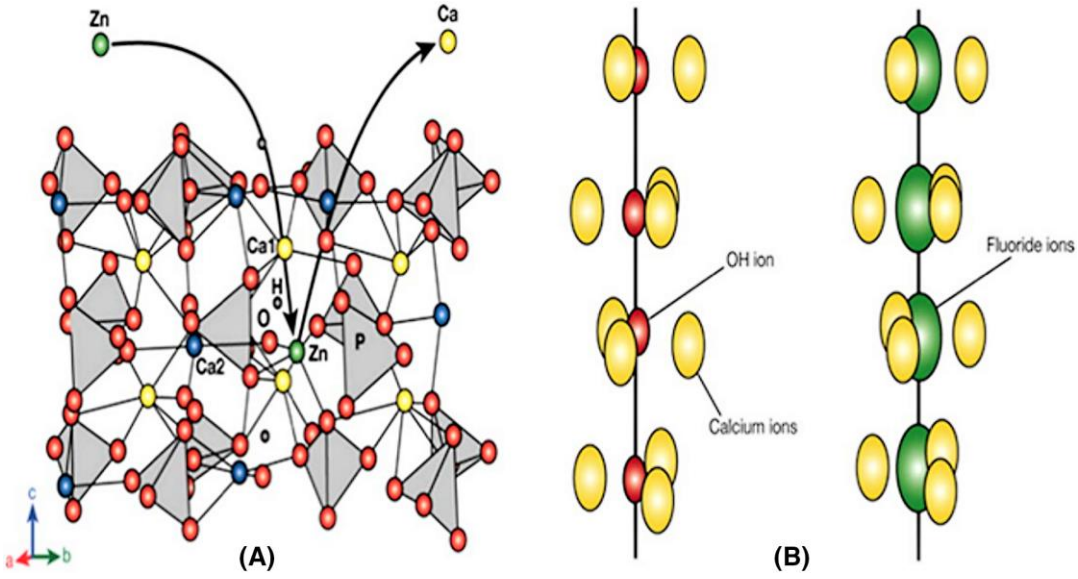

Figure 1.5. Ion substitution within HA structure; A) Cationic substitution, B) Anionic substitution (Cacciotti, 2019)

1.2.1.3 Manganese-doped Hydroxyapatite

Manganese (Mn) is one of the doping elements used in ion doped HA researches. Mn promotes the integrin receptors in terms of their ligand-binding affinity. Integrins are essential in cellular interactions with ECM (extra cellular matrix) and cell surface ligands. The presence of Mn promotes the cell adhesion by increasing the ligand affinity (Bracci et al., 2009; Sopyan et al., 2011). One study showed that manganese reduces bone resorption (Mayer et al., 1993). The addition of Mn at different concentrations can increase the density of HA without changing its phase. Mn can also enhance the binding of the bone (Koksal et al., 2019). Additionally, it has been observed that Mn served as an additive for calcination and sintering of biphasic calcium phosphate without causing the formation of other secondary phases such as CaO and α-TCP. The formation of phases such as α-TCP during sintering, results in the reduced mechanical properties and it stimulated the formation of micro-cracks; hence, it is not preferred to have secondary phases such as α-TCP during sintering process (Ramesh et al., 2007; Sopyan et al., 2011). Kang et al. (2016) indicated that the substitution of Mn in HA lattice, improved osteogenesis and cellular adhesion, and it offered good mechanical properties as a coating for implants (Kang et al., 2016). The Mn concentration range as doping element was reported up to 20 wt % (Kang et al., 2016). In the study done by Kang et al. (2016), increasing the amount of Mn increased the irregularity of the pores and coated surface became denser and micro-cracks could be seen on the surface (Kang et al., 2016). In another study, it was confirmed that the presence of Mn in HA lattice structure as coating material, enhanced the interaction of the implant with the host bone tissue. As indicated in previous studies, Poovendran et al. (2022) also indicated that the Mn-doping HA improved cell adhesion and ligand-binding affinity of surface receptors (Poovendran et al., 2022)

1.2.2 Polymers

The first stage for engineering a biomaterial as bone tissue substitute is the design of a porous 3D scaffold. Polymers are the materials that have proper biodegradability, biocompatibility, and processability features which allow them to be used as base material of bone scaffolds. The size and shape of the polymers can be modified so that the degradation and absorption rates would be kept at a controlled level as the tissue cells would be attached, spread, and increased in numbers within the 3D scaffold structure (Hutmacher, 2000).

Polymers can be divided into synthetic and natural groups in terms of their origin. Natural polymers have natural origins, and the examples are silk, collagen, cellulose, etc. Synthetic polymers are synthesized by engineers and scientists, such as polycaprolactone (PCL), polyglycolide (PGA), polylactides (PLLA, PDLA), etc.

The polymers in the group of poly (α-hydroxy acids) undergo bulk degradation. These polymers have different degradation rates; for example, PDLA and PGA molecular weight decreases after one day of exposure to aqueous media; the molecular weight of PLLA on the other hand decreases after a few weeks upon exposure to aqueous media. The mass loss results in the formation of acidic by-products. The release of acidic by-products can cause inflammatory reactions around the material and decreases in the pH of defected area. The addition of bioceramics like tricalcium phosphate (TCP) or HA can change the degradation and resorption kinetics of the polymeric material. Therefore, the fabrication of polymer/bioceramics composites can enhance the biocompatibility of the material such as buffering the pH of the surrounded area (Hutmacher, 2000).

There are different techniques that can be used for scaffold formation via polymers; one of the widely used techniques is electrospinning. Electrospinning can have different setups such as dry/wet electrospinning, uniaxial, coaxial, multi-axial, needle-based, needleless, and co-electrospinning (Haider et al., 2018).

In needle-based electrospinning, an electrostatic force is drawn in order to help the formation of fibers from the needle tip into the collector. When the electric repulsion in the droplet (at the tip of the needle) overcomes the liquid surface tension, a charged jet forms and causes the formation of a 3D scaffold within the collector (Figure 1.6).

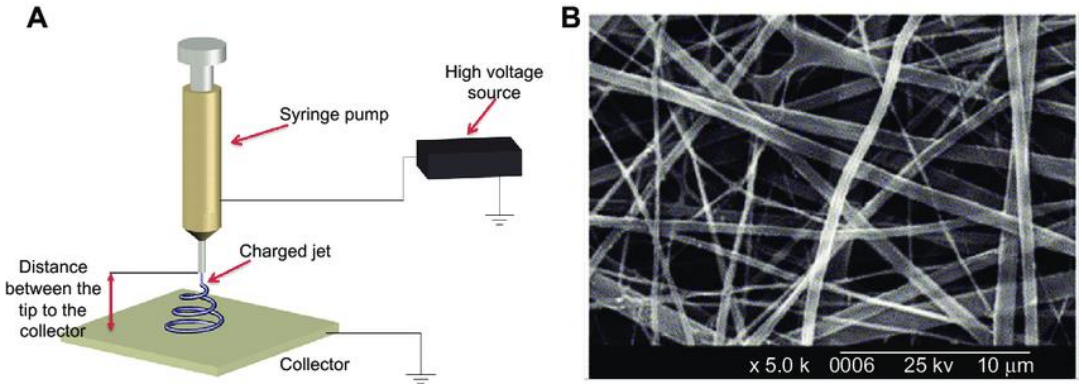

Figure 1.6. Electrospinning setup for scaffold formation (Lu et al., 2013)

1.2.2.1 Poly (ε-caprolactone)

Poly (ε-caprolactone) or PCL is a linear aliphatic polyester with suitable biocompatibility and long degradation time due to its high crystallinity and hydrophobicity (Yedekçi et al., 2022). PCL has been approved by FDA (Food and Drug Administration) for *in vivo* researches and human clinical use. Also, it does not generate any acidic or toxic by-product due to its slow degradation rate. Therefore, it is a proper polymer for bone scaffold formation. Low degradation rate of PCL can be modified by addition of other synthetic polymers such as PLA or PLGA, or bioceramics can be blended to PCL scaffolds as well. Besides that, the addition of bioactive compounds like TCP or HA can enhance osteoconduction of the bone (Ghayor et al., 2020; He et al., 2013). PCL can be combined with natural polymers including collagen and gelatin which can increase biodegradation, wettability and cellular adhesion of the designed scaffold (Yedekçi et al., 2022). Previous literature

studies also showed that PCL/HA composite enhanced hydrophilicity and biological activities of the scaffolds.

PCL has a suitable biodegradability and shape memory properties and it is widely used in as a composite material in scaffolds' fabrication. Due to the shape memory effect, a small-sized PCL implant can be placed in body temporarily and it can fully recover its original shape after being exposed to specific thermal stimulus. However, PCL is unable to carry external loads because of its low strength and hardness; therefore, PCL alone is not preferrable in bone repair applications and fabrication of TE scaffolds. Addition of HA nanoparticles can improve PCL in terms of its mechanical, biological and bioactivity properties. PCL/HA composite enhances cellular adhesion, osteogenic gene expression, and proliferation (Tian et al., 2019).

The natural bone has both organic and inorganic compartments, and polymer-ceramic composite scaffolds have gained interest due to their similarities to natural bone structure. HA enhances biocompatibility, and osteoconductivity of the PCL/HA scaffold. The combination of HA with PCL boosts the final properties of composite material (Wang et al., 2010). One study indicated that the addition of HA within the range of 20-40% increased proliferation ratio of the cells. It also promoted the biomineralization and protein adsorption capacity due to the surface morphology and addition of HA into PCL structure (Li et al., 2021). In another study, PCL/HA scaffold represented suitable mechanical and structural properties over 6 months, and it improved cell adhesion and proliferation (Wang et al., 2010).

1.2.2.1.1 Surface Modification of PCL scaffold

Due to the stable bulk features of polymers, such as resistance to thermal degradation and solvent treatments, they can be used in substitution of metallic-based materials. The surface of the polymers, however, prevent them to be functional and useful in their intended applications. Therefore, surface modification is needed to compensate for their limitations (Nemani et al., 2018).

Surface modifications can be done through two different general methods: 1. chemical or physical alteration of atom and molecules on the surface of material (etching, treatment, or chemical modification), 2. coating the surface by another material that has new composition (chemical grafting, thin film deposition, or solvent coating). Thickness of added layer in surface modification is important; addition of a thick layer changes the mechanical and functional properties of the main material; hence, thin coating layers are more desirable (Ratner, 1995).

Polymers, nanoparticles, organic and inorganic compounds have been proposed as a potential candidate for coating material. Coatings are frequently applied to improve the wettability, cellular adhesion, and corrosion resistant properties of the coated material. For instance, graphene-based materials are one of the best materials for coating due to its barrier properties (Sharma & Sharma, 2021).

The surface of PCL scaffold can be modified through covalent chemical conjugation and non-covalent physical adsorption techniques. The chemical conjugation is through the bonding of COOH, NH_2, and OH^- groups. The examples are surface etching, gamma-ray irradiation, and oxygen plasma treatments. Chemical surface modification provides more stability in terms of the surface attachment; however, the possibility of the creation of toxic by-products is its drawback for biomedical usage. Other than providing biocompatible surface for cell attachment and growth, the coating material should also include the signaling growth factors in order to mimic the surface of the natural bone. The surface modification of PCL by bone morphogenic protein 2 (BMP-2) is one way to increase the biocompatibility of PCL scaffold in terms of cell adhesion and proliferation (Qin et al., 2022).

1.2.2.2 Collagen/Gelatin

Collagen, the main protein of organic part of the bone, regulates specified mechanical properties such as flexibility, toughness, and strength. The interaction of collagen with mineral phase of the bone regulates the mechanical properties of the

bone; the mineral phase or HA itself is responsible for the stiffness of the bone structure. Since collagen is one of the main components of bone structure, it has been used as a prominent material for bone tissue engineering since 1900s. There have been trials to substitute gelatin (or similar molecules) with natural collagen due to the limitations and difficulties for obtaining and use of collagen as a suitable biomaterial (Mallick et al., 2022).

Collagen has a great healing ability, and it can be used in minor or major bone tissue defects. Hence, due to its abundance and healing ability, it is still an excellent choice to be used in bone tissue engineering field. The micro and macrostructure of the biomaterial surface plays an important role in osteoconductivity, osteoinductivity, and osteointegration for bone healing. Osteoconduction is defined as the growth of host progenitor cells on the surface of the implant for bone repair. Osteoinduction is the recruitment of immature bone cells and their growth stimulation. Osteointegration is expressed as the development of direct contact between the host tissue surface and the implant in order to give a stable anchorage for the implant inside the body. These three phenomena are very crucial for the repair and growth of bone tissue in defective areas. Other factors such as degradation and mechanical properties of the biomaterial have an important role in bone repair and regeneration. The degradation rate should match the regeneration rate of the tissue in order to obtain suitable cell proliferation with no lack of nutrient supply so that the tissue would regenerate properly within the scaffold. The combination of type I collagen with elastin, gelatin, or other types of collagen, can improve the mechanical properties and rate of degradation when implanted in natural bone tissue (Mallick et al., 2022).

Gelatin is a biopolymer made when collagen is thermally denatured or degraded physically and chemically. Due to the biodegradability and biocompatibility properties of gelatin, it is frequently used in different TE applications. In contrast to its precursor, gelatin is nonimmunogenic and encourages cell adhesion, migration, proliferation, and differentiation. Additionally, gelatin quickly undergoes chemical

cross-linking with the use of cross-linkers because of the abundance of the functional groups, which is crucial for its usage as a biomaterial (Choi & Kim, 2012).

1.2.3 Composite Materials

Composite material is referred to a combination of two or more materials with different compositions and morphologies on a macroscopic scale, in order to achieve a particular chemical, physical, or mechanical properties. The composite material is usually intended to show the best properties of its components and some useful and specified properties that the constituent parts lack (Nicolais et al., 2010).

For instance, PCL/HA composite scaffolds are widely used in bone tissue engineering due to the proper biological and mechanical properties that the scaffold provides. Due to the hydrophobicity feature of PCL, it is insoluble in water, and it degrades in the body very slowly; this feature can be both advantageous and disadvantageous. Low solubility of PCL can keep the drug trapped in microsphere for a long duration in drug delivery applications. In bone tissue applications, however, the degradation rate of the PCL scaffold should match the regeneration rate and due to this important factor, PCL is generally combined with another polymer or bioceramics material to form composites (Yedekçi et al., 2022).

1.3 Aim of the Study

The goal of this study was to develop gelatin-coated 3D PCL scaffold incorporated with pure and manganese-doped HA for BTE applications. The effect of gelatin coating in the structural and biological properties, and the effect of Mn doping in the bone formation, osteoconduction, and bioactivity of the primary PCL scaffold for BTE was investigated. The composite scaffold was fabricated by the wet electrospinning of PCL scaffold together with Mn-doped HA was done for the first time in literature. The cross-linking of a thin gelatin coat around these PCL fibers to

obtain the final PCL/gelatin/Mn-HA scaffold to analyze its properties as a BTE scaffold was also done for the first time with this thesis study.

CHAPTER 2

MATERIALS AND METHODS

2.1 Materials

Calcium nitrate tetrahydrate ($Ca(NO_3)_2.4H_2O$) (Merck, Germany) and diammonium hydrogen phosphate ($(NH_4)_2HPO_4$) (Merck, Germany) was used in order to synthesize pure HA. Mn-doped HA samples required additional precursors (compounds) for their synthesis; Manganese (II) sulfate monohydrate ($MnSO_4.H_2O$) (Merck, Germany) and manganese (II) chloride ($MnCl_2.4H_2O$) (Riedel-De-Haën, Germany) were used to synthesize manganese-doped hydroxyapatite samples (Mn-HA). Ammonia solution (NH_4OH) (Merck, Germany) was used for the pH adjustment of HA and Mn-HA during their synthesis.

Poly (ε-caprolactone) (pure, Mn: 80,000, 97%, Sigma-Aldrich, USA), gelatin type A (from porcine skin, gel strength 300, Sigma-Aldrich, USA), glutaraldehyde (Merck, Germany), glycine (Sigma-Aldrich, USA), chloroform (Merck, Germany), and acetone (pure, <=100%, Merck, Germany) were used for preparation of scaffolds.

For cell culture studies, the following materials were used for different analysis: High glucose Dulbecco's modified Eagle medium (DMEM) (Merck, Germany), fetal bovine serum (FBS) (Biological Industries, USA), penicillin/streptomycin (Biological Industries, USA), Trypsin, Trypan Blue, Alamar Blue™ (Invitrogen, USA), picogreen (Invitrogen, USA), and pNPP (Sigma-Aldrich, USA). Moreover, hexamethyldisilane (Sigma, USA), paraformaldehyde powder (Sigma, USA), hydrochloric acid (HCl) (Merck, USA), and sodium hydroxide (NaOH) (Merck, Germany) were used for cell fixation.

2.2 Methods

2.2.1 Synthesis and Characterization of HA and Manganese-doped HA

2.2.1.1 Synthesis of HA and Manganese-doped HA

Pure HA and Mn-doped HA were synthesized by microwave irradiation (Alshemary et al., 2013). The main precursors of HA synthesis are calcium nitrate tetrahydrate ($Ca(NO_3)_2.4H_2O$) as Ca^{2+} source and diammonium hydrogen phosphate ($(NH_4)_2HPO_4$) as PO_4^{3-} source. Calcium nitrate (1.0M) and diammonium hydrogen phosphate (0.6M) were dissolved separately in 200 ml distilled water (dH_2O). After complete dissolution of the mentioned precursors in dH_2O, the ammonium phosphate solution was added dropwise to the calcium nitrate solution while it is continuously stirred by magnetic stirrer under chemical fume hood. The solution pH was kept constant around 10 by the addition of ammonia solution (NH_4OH). After complete addition of ammonium phosphate solution into the calcium solution (at room temperature), the resulting mixture was stirred for an additional 30 minutes. While stirring, the mixture pH was adjusted by NH_4OH and kept constant around 10. Then, the mixture was placed in a microwave oven for 15 minutes at 800W. After this step, the mixture was filtered and washed with dH_2O in order to decrease the pH to 7-8 (biological pH). The excess water and ammonia from the resulting precipitate was removed by drying it overnight at 100°C. The dried samples were sintered in a furnace (Protherm Furnaces, Turkey) at 800, 900, and 1000°C for 2h.

For the Mn-doped HA samples, the synthesis steps are similar to the synthesis of pure HA. The only difference is the addition of 2mol% Mn powders ($MnSO_4.H_2O$ and $MnCl_2.4H_2O$) along with calcium nitrate powder. Two different Mn sources were used in order to examine their effect on structural and biological properties of the Mn-doped HA for choosing the superior one as the Mn source for later experiments. During this step, manganese powders were dissolved in dH_2O initially,

and then calcium nitrate powder was added (for dissolution) to the same solution. The setup for HA (and Mn-HA) synthesis procedure is seen in Figure 2.1.

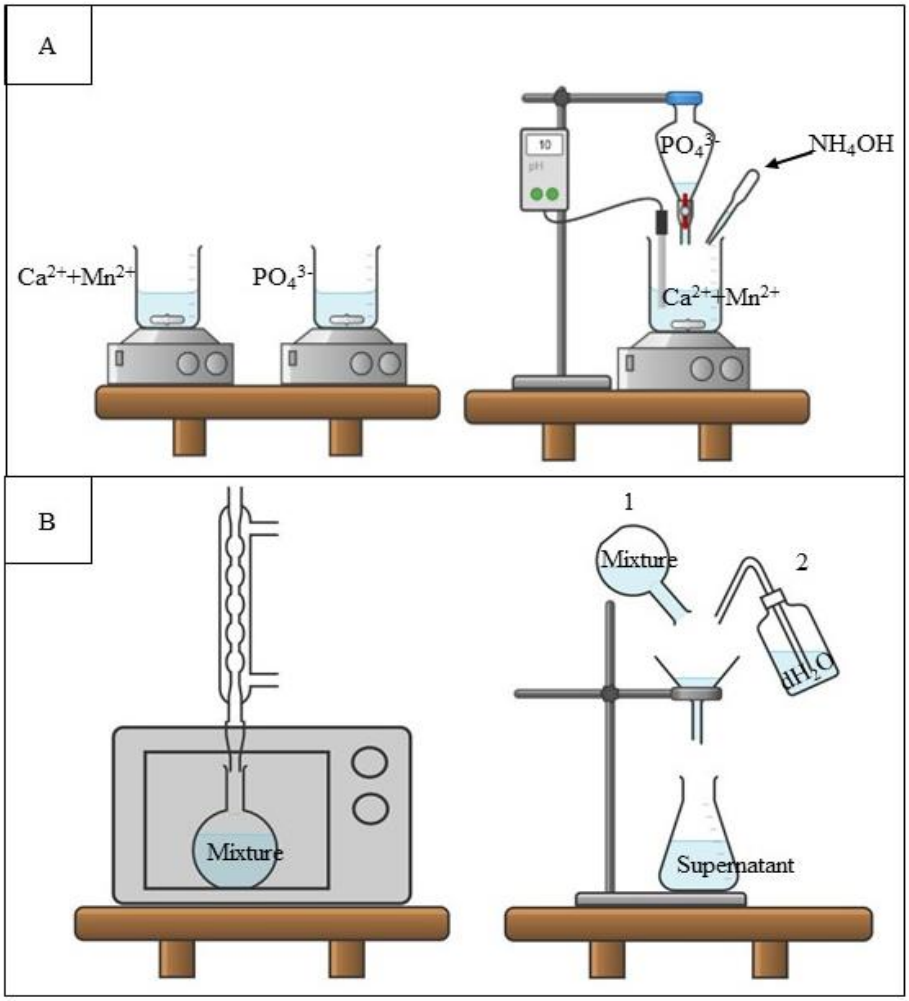

Figure 2.1. Syhthesis steps of HA; A) Dissolutions of precursors, and drop-wise addition of phosphate solution into calcium (or calcium/manganese) solution, B) Microwave irradiation, followed by washing and filtering steps

2.2.1.2 Structural Characterizations

2.2.1.2.1 X-Ray Diffraction Analysis (XRD)

XRD analysis was done to identify the phases present in HA and Mn-doped HA after synthesis. Rigaku Ultima IV X-Ray diffractometer (Central Lab, METU) was the device used for XRD analysis. This device utilizes the Cu-Kα radiation at 40kV and 30 mA, and the scan rate and step size were fixed at 2°/min and 0.02°, respectively. The Joint Committee on Powder Diffraction Standards (JCPDS) files were used to compare the positions of diffracted planes (with the standards).

The percentage of hydroxyapatite and β-TCP phases of each sample were calculated by the relative intensity ratio (RIR) (Equation 1). In Equation 1, I_{HA} and $I_{\beta\text{-TCP}}$ indicate the normalized intensities of HA and β-TCP, (2 1 1) and (2 0 1 0) peaks, respectively (Farzadi et al., 2011).

$$RIR = I_{\beta\text{-}TCP} / (I_{\beta\text{-}TCP} + I_{HA}) \qquad (1)$$

The degree of crystallinity of crystalline phases which were present in the analyzed volume of XRD spectra was calculated by Equation 2.

$$X_c = 1 - (V_{112/300}/I_{300}) \qquad (2)$$

In Equation 2, X_c indicates the degree of crystallinity, I_{300} is the intensity of (3 0 0) reflection, and $V_{112/300}/I_{300}$ is the intensity of the hollow between (1 1 2) and (3 0 0) diffraction. MDI Jade 6, Origin, and Highscore plus software were used to analyze the lattice parameters (a and c), degree of crystallinity and phase percent of each group.

2.2.1.2.2 Fourier Transform Infrared Spectroscopy (FTIR)

The FTIR spectra was used to determine the chemical composition, types of bonds and changes/shifts in absorption bands of synthesized HA and Mn-doped HA groups. A spectrophotometer is used to record the FTIR spectrum from 4000 cm^{-1} to 400 cm^{-1} by performing 100 scans on the spectrophotometer device (Perkin Elmer, Inc., UK, Central Lab, METU).

2.2.1.2.3 Inductively Coupled Plasma-Mass Spectroscopy (ICP-MS)

Inductively coupled plasma-mass spectroscopy (ICP-MS, Perkin Elmer Plasma 400, Central Lab, METU) was used to verify and measure the percentage of the elements within the samples, and the ratios of calcium to phosphate (Ca/P ratios) were calculated by using the ICP data. The ICP results of Mn-doped samples were compared with their theoretical values (2 mol%) to verify the presence and the amount of doped Mn element within Mn-HA groups.

2.2.1.2.4 Scanning Electron Microscopy (SEM)

SEM analysis was done in order to characterize and determine the morphology and the particle size of pure HA and Mn-doped HA particles. Quanta 400F Field Emission SEM, USA with a resolution of 1.2 nm was the device used for SEM analysis. The samples were initially mounted onto the metal stubs with the help of carbon tapes, and Hummle VII sputter coating device (Anatech, USA, Central Lab, METU) device was used for vacuum-coating the samples with gold for SEM analysis.

2.2.1.2.5 Indirect Cytotoxicity Test of Synthesized HA and Mn-HA

The indirect cytotoxicity method was used to measure the toxicity of HA and Mn-doped HA on cells. L929 cell type was used in the cytotoxicity studies (Sarasua et al., 2011). Initially, L929 cells were grown in high glucose DMEM enriched with 10% FBS, 1% penicillin/streptomycin and 1% sodium pyruvate. The cells were poured in a T-25 flask containing DMEM media and kept in a carbon dioxide incubator (5% CO_2, 5215 Shel Lab., Cornelius, OR, USA), and awaited at 37°C for 2-3 days. When they reached 80% confluency, cells were removed from the flask using 0.1% Trypsin/EDTA solution. The cells were counted by using a hemocytometer, and 5×10^3 cells/well were seeded in 96 well plate. HA and Mn-doped HA powders were sterilized by heating in furnace at 200°C for 2h. The powders were poured in cell growth media (high glucose DMEM media) with the concentration of 0.2g/ml (Iso, 2012) and incubated in water bath at 37°C for 24h, in order to make extractions for each powder sample. After 24 hours of cell seeding, the extracts of HA, and the two groups of Mn-HA (Mn-sulfate and Mn-chloride) with 4 different dilutions (1, 1/2, 1/4, 1/8) were added to each well (n = 5) and the control group was cells grown with normal cell culture media. The Alamar Blue test was done to measure the cytotoxicity of the powders on L929 cells. Seeded cells were incubated at 37°C in incubator (5% CO_2, 5215 Shel Lab., Cornelius, OR, USA), and the test was done after 24 and 48h of addition of powder extracts to each well.

2.2.2 Synthesis and Characterization of PCL Scaffold

2.2.2.1 Synthesis of PCL Scaffolds and PCL/HA and PCL/Mn-HA Composite Scaffolds

The PCL solution was made by the addition of PCL beads (M_w = 80,000) to the chloroform-acetone solvent system with 3:1 ratio (chloroform: acetone). The PCL is initially dissolved in chloroform for 30-45 minutes on magnetic stirrer and then

acetone is added to the solution. For the composite scaffolds, pure HA or Mn-doped HA powders are added at the last step (after addition and mixture of acetone with the solution). The solution is stirred continuously during the whole procedure (without heating). The PCL solution was made at 10, 15, and 16% (w/v) concentrations, and HA and Mn-doped HA were added to the solutions with the concentrations of 2.5 and 5% (wt.).

PCL scaffolds were obtained by wet electrospinning method (by the setup shown in Figure 2.2). Each PCL solution was put in a syringe; the tip of the syringe was flattened before. The syringe tip was connected to a voltage source (ES30, Gamma High Voltage Research, Inc., USA) by a clipped wire. The syringe is placed in a syringe pump (New Era Pump Systems, USA), and the solution is pumped out of the tip to a wet collector (water-ethanol bath with 1:1 ratio). The flow rate, voltage, and the needle tip to collector distance should be optimized to produce proper 3D fibrous scaffold structures. The flow rate and voltage were set at 0.6 ml/h and 20kV, respectively. The distance between the needle tip to the collector was fixed at 10cm. The following scaffolds were obtained by wet electrospinning method: 10% (w/v) PCL, 15% (w/v) PCL, 16% (w/v) PCL, 15% PCL + 2.5% (wt.) HA, 15% PCL + 5% (wt.) HA, 15% PCL + 2.5% (wt.) Mn-HA, 15% PCL + 5% (wt.) Mn-HA. The obtained scaffolds were placed in -80°C overnight and then freeze dried for 48h.

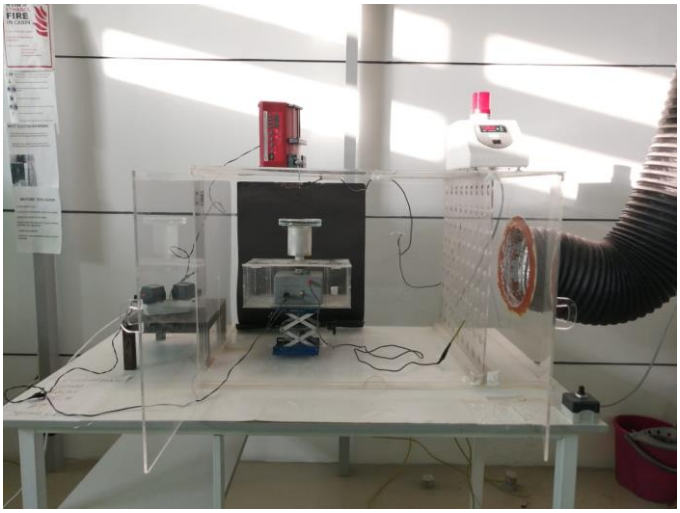

Figure 2.2. Wet electospinning setup

2.2.2.2 Gelatin-Coated PCL/HA and PCL/Mn-HA Composite Scaffolds

The PCL-HA and PCL/Mn-HA scaffolds were crosslinked with gelatin type A (from porcine skin) through the following steps:

The 5% (w/v) gelatin solution was prepared by the addition of the gelatin powder to the beaker containing dH_2O at 37-38°C and constant stirring for 2h. A urine cup was used as the container for gelatin coating; since the PCL scaffold has a low density, it should be kept in the middle so that the gelatin would be coated on the top and bottom properly (with relatively equal thickness). For preparing the setup, the bottom of the cup was completely removed and replaced with parafilm so that the gelatin would be removed easily after the crosslinking procedure is done. In order to keep the scaffold in place, the cup was pierced from four sides in order to put a thread through (as a square shape). Figure 2.3 shows the bottom and the top view of the setup.

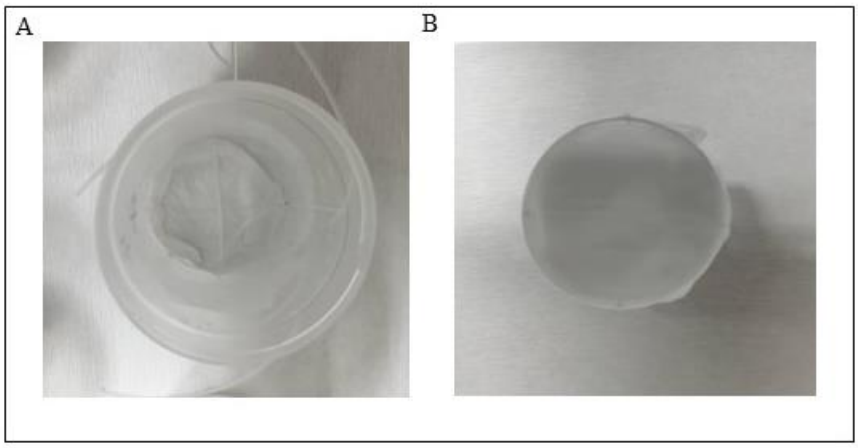

Figure 2.3. Top and bottom view of the setup for gelatin coating and cross-linking around PCL electrospun scaffolds; A) bottom view showing parafilm covering the bottom of container, B) top view showing the scaffold held by the threads from four sides

Five groups of scaffolds were coated with gelatin (the optimized scaffolds): 15% PCL, 15% PCL + 2.5% HA, 15% PCL + 5% HA, 15% PCL + 2.5% Mn-HA, and 15% PCL + 5% Mn-HA. Each of these scaffolds were placed in a separate container

(the setup shown in Figure 2.3) and 10ml gelatin solution was added to each scaffold (Figure 2.4).

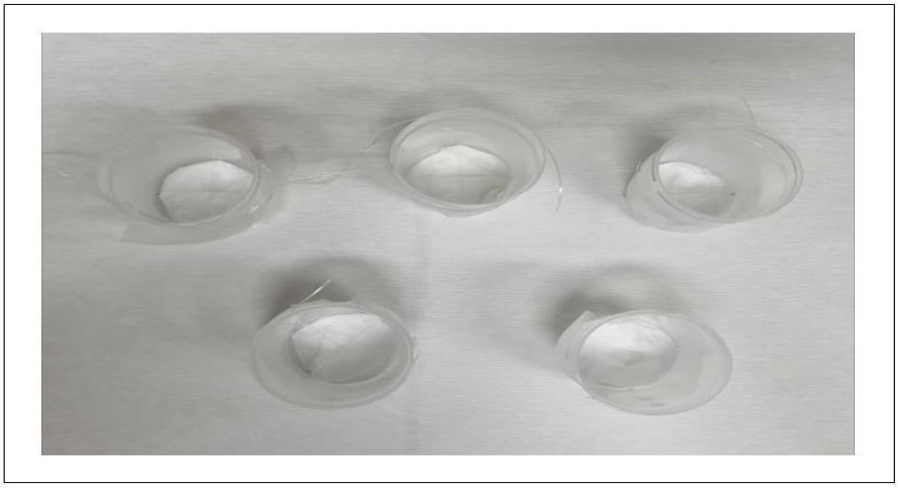

Figure 2.4. Five scaffolds placed in each container, before addition of the gelatin solution.

After the addition of the gelatin solution, the scaffolds (inside the containers) were placed in incubator for two hours (the incubator temperature was 37°C, to keep the gelatin solution liquid) in order to imbibe gelatin solution towards inside of the scaffold.

At the end of this period, the PCL scaffolds were completely soaked and immersed in gelatin. Then, they could be crosslinked. After adding 1% Glutaraldehyde (GTA) to each scaffold containing solution, each container was shaken initially by hand (for homogenous dispersion of the GTA), and then they were placed on shaker inside the incubator for at least 30min (at 150-180 rpm).

After 30 minutes, the scaffolds were taken out from the incubator and off the shaker and were kept at room temperature for another 30min for complete cross-linking (gelation) of the gelatin (Figure 2.5). Then, the cross-linked scaffolds were gently removed from their containers and washed with glycine solution (0.2 M) for 1h (on shaker at 150 rpm, at room temperature). After glycine wash, the scaffolds were

washed with dH_2O for 1h (on shaker at 150 rpm, at room temperature). After the washing steps, the scaffolds were placed in deep freezer at -80°C and then freeze dried (Figure 2.5).

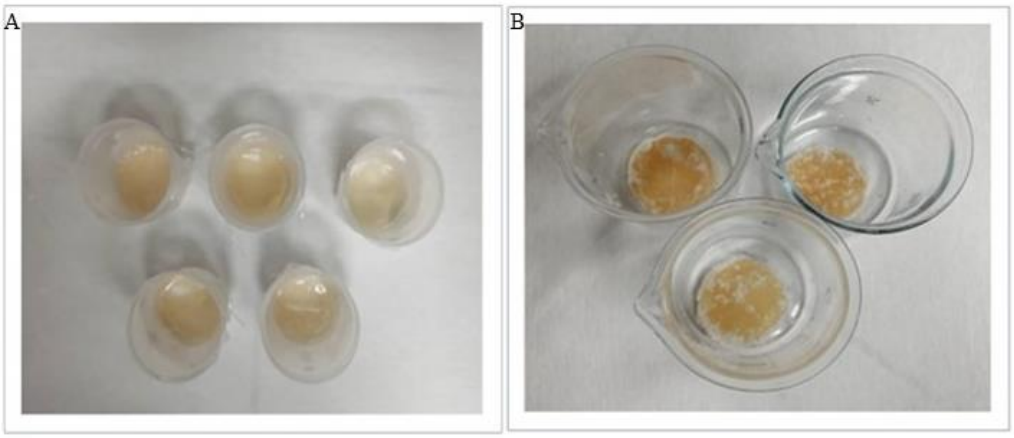

Figure 2.5. Crosslinked gelatin coated PCL scaffolds; A) before washing steps, B) After washing and freeze drying

The freeze-drying step was done in two separate stages; first the scaffolds were freeze dried for 4-5h, then the scaffolds were punched into smaller samples (7mm diameter punch). The small samples were washed again with glycine solution (0.2 M) and dH_2O for 1hr for each washing step (like the previous washing protocol). At the end, the scaffolds were freeze dried for 14-16h to make sure they were dried completely (Figure 2.6). The thickness of the top and bottom gelatin layer of each scaffold was about 2 mm, and the overall thickness of the final scaffold was 5-6 mm. The scaffolds were further used for different characterizations and analysis.

Figure 2.6. Final gelatin coated scaffolds, after 14-16 h of freeze drying

2.2.2.3 *In Vitro* Degradation analysis

In-vitro degradation analysis was done on PCL/gelatin/HA, and PCL/gelatin/Mn-HA scaffolds (n=3). The test was done in 12 ml PBS solution (pH = 7.4, 0.01M) for 1, 7, 14, and 21 days, in shaking water bath at 37°C. Before starting the degradation test, the initial dry weight was measured for each scaffold. Then, the scaffolds were placed in 15ml falcon tubes containing 12ml PBS solution. At each time point, the wet weight of scaffolds was measured for water uptake analysis. The dry weight of each scaffold was measured on day 1, 7, 14, 21 after freeze drying for at least 14hr (to make sure no moisture is left). Equation 3 is used for calculating the weight loss percentage of each scaffold:

$$\text{Weight loss (\%)} = (M_i - M_f / M_i) \times 100 \qquad (3)$$

In Equation 3, M_i and M_f represent the initial and final dry weight of scaffolds at each time point.

The water uptake analysis was also done for each scaffold at 1, 7, and 14, and 21 days. The scaffolds (n=3) were immersed in 12ml PBS solution. At each time point, the scaffolds were washed with dH_2O and placed on shaker for 2hr. Then, the excess water of each scaffold was removed by filter paper, and the wet weight of each

scaffold was calculated with Equation 4. In Equation 4, W_w indicates the wet weight, and W_i represents the initial dry weight of each scaffold.

$$\text{Water uptake (\%)} = (W_w - W_i / W_i) \times 100 \quad (4)$$

2.2.2.4 *In Vitro* Bioactivity Test

Simulated body fluid (SBF, pH = 7.4) was used for bioactivity test and it is prepared by the (modified) Kokubo's method (Kokubo and Takadama, 2006). The SBF solution is made by addition of certain components (chemicals) to 1L dH_2O. Table 2.1 shows the components and their order of addition to produce SBF solution. The components mentioned in Table 2.1, are added sequentially to 1L dH_2O at room temperature and constant stirring. The SBF solution was prepared in a plastic beaker to avoid crystal formation. It is important to keep the temperature and pH of SBF solution at a specific range according to Kokubo's method (Kokubo and Takadama, 2006) in order to avoid crystal formation.

Table 2.1. SBF solution components for preparation of 1L solution

Order of addition	**Components**	**Added amounts**
1	NaCl	8.035 g
2	$NaHCO_3$	0.355 g
3	KCl	0.225 g
4	$K_2HPO_4.3H_2O$	0.231 g
5	$MgCl_2.6H_2O$	0.311 g
6	1.0 M-HCl	39 ml
7	$CaCl_2$	0.292 g
8	Na_2SO_4	0.072 g
9	Tris	6.118 g
10	1.0 M-HCl	0-5 ml

Each scaffold (n=3) was placed in a 15ml falcon tube (polypropylene container) and incubated at 37°C in incubator, for 7 and 14 days. The amount of SBF used for each scaffold was calculated by Equation 5. In Equation 5, V_s (ml) is the volume of SBF used for incubation of each scaffold, and S_a is the surface area of the scaffold (mm^2). Hence, the 12ml SBF was added to each 15ml falcon tube (based on Equation 5).

$$V_s = S_a/10 \quad (5)$$

At each time point (Day 7 and 14), the SBF was discarded, and each scaffold was rinsed with dH_2O and freeze dried for at least 14h (until no moisture is left). The SEM and EDX analyses were done on dried scaffolds (at the end of each time point) in order to evaluate the formation of apatite layer (mineralization) on each scaffold's surfaces. The Ca/P ratio was calculated by the Calcium and phosphates peak intensities obtained from EDX analysis. Also, the pH of the SBF solution was measured by a pH meter (S20 SevenEasy^{TM} pH) every 2 days and at the end of each time point (day 7 and 14).

2.2.2.5 Cell Culture Analysis

For cell culture analysis, Saos-2 (Human bone osteosarcoma) cells were used. These cells were grown in cell growth medium containing high-glucose DMEM, 10% FBS, 1% penicillin/streptomycin, and 1% sodium pyruvate, and they were incubated in a CO_2 incubator at 37°C (5% CO_2, 5215 Shel Lab, Cornelius, OR, USA). After the cells reached 80% confluency, they were sub-cultured into a bigger flask. At this step, the cells were detached by 0.1% Trypsin/EDTA solution. Before seeding the cells, the scaffold should be sterilized. For sterilization step, the scaffolds were initially incubated in 70% absolute ethanol solution for 2h. Then, the ethanol was discarded, and each side of the scaffolds was exposed to UV irradiation for 30min. After this step, cell growth media was poured into each well (on each scaffold), and the samples are incubated for 24 h (to make sure that ethanol is completely removed from the scaffolds).

2.2.2.5.1 Alamar Blue™ Cell Viability Test (Direct Cytotoxicity)

The Saos-2 cells were seeded on the surface of the gelatin-coated PCL and PCL scaffolds at a density of 1×10^4 cells/scaffold. These seeded scaffolds were incubated at 37°C for 7 days in CO_2 incubator (Shell Lab, USA). The AlamarBlue™ test was done to measure the viability of cells at different time points (day1, 4, and 7). At each time point, after removal of the cell growth medium, the scaffolds were washed with PBS, and then AlamarBlue™ solution (10% Alamar Blue™ reagent in 90% DMEM without phenol red) was added to each well (containing scaffold). The Alamar Blue™ media were collected from each well after 4h of incubation, and the absorbance was read at 570 and 600 nm with a microplate reader (Module 9200, Turner Biosystem, USA). After this step, the cells were washed again with PBS and fresh cell growth media were added for incubation of the scaffolds for the next time point. The cell viability (%) was calculated by the Equation 6:

$$\left(\frac{(O2\times A1)-(O1\times A2)}{(R1\times N2)-(R2\times N1)}\right)\times 100 \qquad (6)$$

In Equation 6, O_1 and O_2 represent the molar extinction coefficient (E) of the oxidized Alamar Blue at 570 and 600 nm. A_1 and A_2 are the absorbance of the test wells at 570 and 600nm. R_1 and R_2 indicate the molar extinction coefficient (E) of reduced Alamar Blue at 570 and 600nm. N_1 and N_2 are the absorbance of negative control wells at 570 and 600nm. The gelatin coated scaffolds without cells were used as negative control for each group. The relative cell viability (%) can be calculated by Equation 7, considering the control group as 100%.

$$\text{Relative cell viability (\%)} = (\text{Viability}_{\text{test}} / \text{Viability}_{\text{control}}) \times 100 \qquad (7)$$

2.2.2.5.2 Osteogenic Activity of Cells

Alkaline phosphatase (ALP) activity of cells was measured in order to evaluate the osteogenic activity of Saos-2 cells on gelatin coated scaffolds (n=5). The gelatin

coated scaffolds were used as negative control for each group. 2×10^4 cells were seeded on each scaffold. The scaffolds were initially seeded on scaffolds within cell growth media. The media was replaced by osteogenic differentiation media (High glucose DMEM containing 10%FBS, 1% penicillin/streptomycin, 50µg/ml ascorbic acid, 10 mM β-glycerophosphate, and 10^{-8} M dexamethasone). The scaffolds were incubated in osteogenic media for 7 and 14 days. The osteogenic media was renewed every 3 days. At the end of each time point, the cells were lysed by 3 cycles of freeze/thawing. Triton X 100 (1%) was diluted 10 times by carbonate buffer (0.2M) in order to prepare the cell bursting solution. The cells were washed with PBS initially, and 300 µL of triton X 100 (0.1%) was added to each well for bursting the cells in freeze/thawing cycles. The obtained cell lysates were used for ALP test. pNPP working solution was prepared by mixing pNPP substrate solution (p-nitrophenyl phosphate), $MgCl_2$ (100mM) solution, and dH_2O with 10:1:20 volume ratio. Lysate (50 µL) and PNPP working solution (100 µL) was added to a 96 well plate and incubated for 1h at 37°C. The absorbance was read at 405nm with a microplate spectrophotometer (µQuant MQX200, Biotek, USA). BCA (Bicinchoninic acid assay) was used for measuring total amount of protein in the lysates (Lozzi et al., 2008). Cupric acid (4%) was mixed with bicinchoninic acid (BCA reagent) in 1:50 volume ratio in order to prepare BCA working solution. Lysate (25 µL) and BCA working solution (175 µL) were added to a 96 well plate and incubated for 1h at 37°C. The absorbance of samples for BCA test was read at 562nm with a microplate spectrophotometer (µQuant MQX200, Biotek, USA). For ALP and BCA data, two calibration curves were constructed by using 4-nitrophenol and BSA (bovine serum albumin) solutions, respectively. Different concentrations were used for 4-nitrophenol solution (0-16384 µM) and BSA solution (0-512 µM). By using calibration curves of ALP and BCA with known concentrations, the total amount of 4-nitrophenol and protein produced can be measured, respectively. To determine specific ALP activity of cells, the ALP activity was normalized by protein content.

CHAPTER 3

RESULTS AND DISCUSSION

3.1 Characterization of Pure and Manganese-doped Hydroxyapatite (HA and Mn-HA)

3.1.1 Structural Characterization

3.1.1.1 X-Ray Diffraction Analysis

XRD analysis is done to show characteristics of crystalline phases of the analyzed structure. XRD patterns of the pure and Mn-doped HA samples (with two different precursors i.e., Manganese sulfate and Manganese chloride) are shown in Figure 3.1. Pure and Mn-doped HA samples are sintered at three different temperatures, which are 800, 900, and 1000°C for 2h. The XRD patterns of pure and Mn-doped HAs are in acceptable agreement with the standard HA peaks (JCPDS PDF #09-0432). It shows that HA is properly formed in all HA and Mn-HA samples (Table 3.1). By comparing the XRD patterns of HA and Mn-HA samples with the standard β-TCP pattern (JCPDS PDF #09-0169), it can be seen that β-TCP has formed in all Mn-doped groups, except HA-MC-800 group. Similar to the previous studies (Fuh et al., 2017; Kaya et al., 2021), as the sintering temperature increases in different HA samples, the intensity of the peaks increases, indicating the formation of more crystalline HA and Mn-HA structure (Table 3.2). Intensity of the β-TCP peaks increase by increasing the sintering temperature, which was recorded in previous studies (Fuh et al., 2017; Guo et al., 2003); this shows that the sintering temperature affects the peak intensity of all phases in HA and Mn-HA samples. Despite the formation of β-TCP as a secondary phase, HA dominates as the major phase in all

HA and Mn-HA samples. As seen in Figure 3.1, peaks related to the β-TCP phase are highlighted with red dotted line; β-TCP peaks can mainly be detected at 31.026°, 34.371°, 49.785°, 52.944°, and 54.405°. In a previously reported study, some peaks related to the β-TCP phase were identified at temperatures above 1000°C (Fuh et al., 2017).

Greater peak intensities or narrower peaks in samples sintered at higher temperatures (900 and 1000°C) show that these samples have more crystalline structures than samples sintered at 800°C (Kaya et al., 2021).

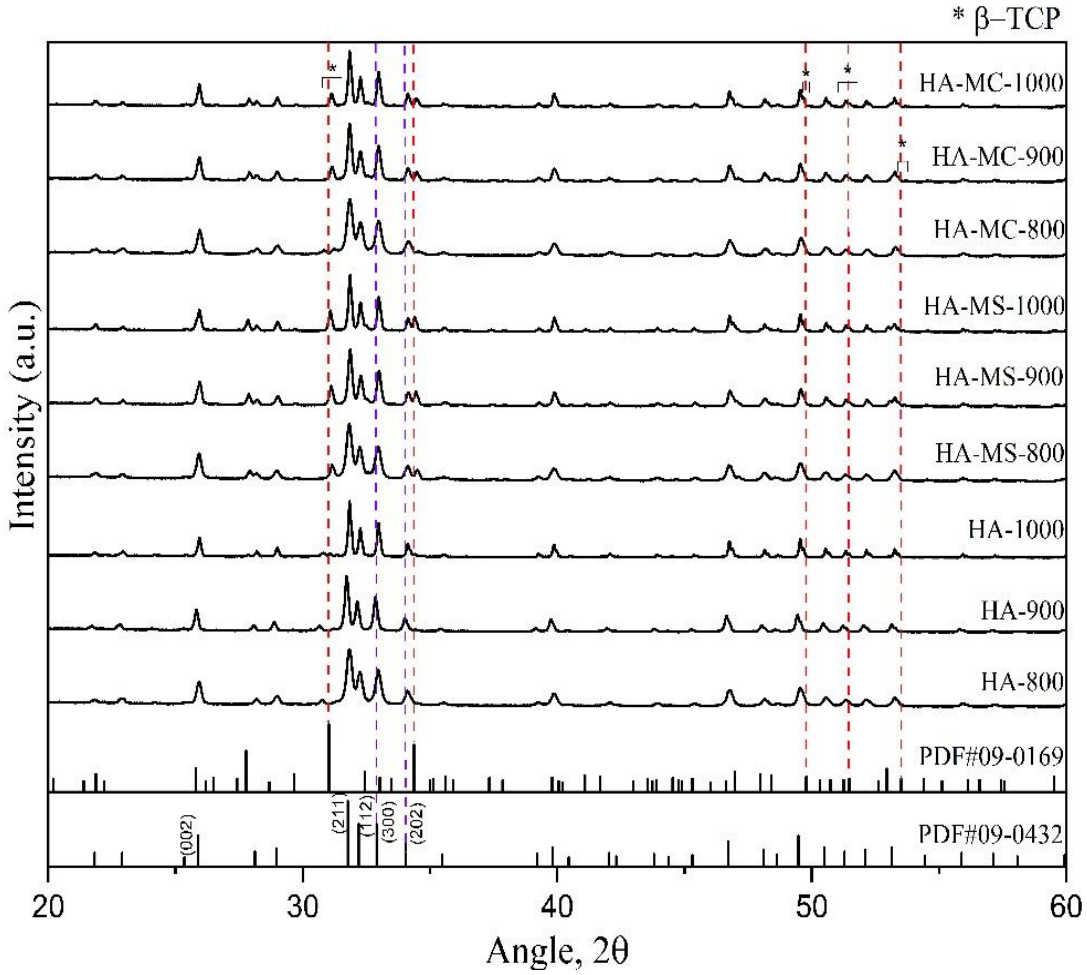

Figure 3.1. XRD patterns of the samples sintered at 800 °C, 900 °C, and 1000 °C, with two different precursors (HA-MS: $MnSO_4$ and HA-MC: $MnCl_2$). Vertical lines indicate the peaks of standard HA (JCPDS PDF#09-0432), and β-TCP (JCPDS PDF#09-0169)

Table 3.1. Phase amounts in HA and Mn-doped HA samples (with $MnSO_4$ and $MnCl_2$ precursors)

Sample	Phase Percentage (%)					
	800°C		900°C		1000°C	
	HA	β-TCP	HA	β-TCP	HA	β-TCP
HA	99.50	0.50	99.80	0.20	90.50	9.50
Mn-HA ($MnSO_4$)	84.30	15.70	75.30	24.70	73.90	26.10
Mn-HA ($MnCl_2$)	93.20	6.80	82.50	17.50	80.70	19.30

Table 3.2. Calculation of degree of crystallinity of HA and Mn-doped HA samples (with $MnSO_4$ and $MnCl_2$ precursors)

Sample	Degree of Crystallinity (%)		
	800°C	900°C	1000°C
HA	83.94	85.87	88.14
Mn-HA ($MnSO_4$)	89.62	90.06	90.40
Mn-HA ($MnCl_2$)	89.41	91.73	92.14

Figure 3.2 indicates the XRD patterns of Mn-doped (sulfate) HA at 2% and 5% (mol) concentrations. As the Mn concentration increased, HA peaks became sharper and narrower, indicating a crystallinity increase in Mn-HA samples (Table 3.4). As mentioned, the β-TCP peaks can be seen in pure and Mn- doped HA samples. β-TCP peaks become sharper and narrower as the concentration of Mn increases from 2% to 5% (mol) (Table 3.3). According to a study on the calcinations of Mn-doped HA samples from 500 to 900°C, the peaks related to the β-TCP phase appear initially at 800°C. As the Mn concentration increases to 10-15% (mol), the peak intensity of the β-TCP phase decreases gradually. This can be due to the replacement of manganese with calcium ions in the β-TCP phase (Natasha et al., 2008). An earlier EPR (electron paramagnetic resonance) spectroscopy study confirmed that Mn ion could partially occupy the Ca^{2+} sites in the β-TCP phase. Atomic radius of the manganese is greater than calcium leading to a decrease in β-TCP peak intensity as the number

of substituted Ca ions with Mn ions increases in the β-TCP phase (Mayer et al., 2006).

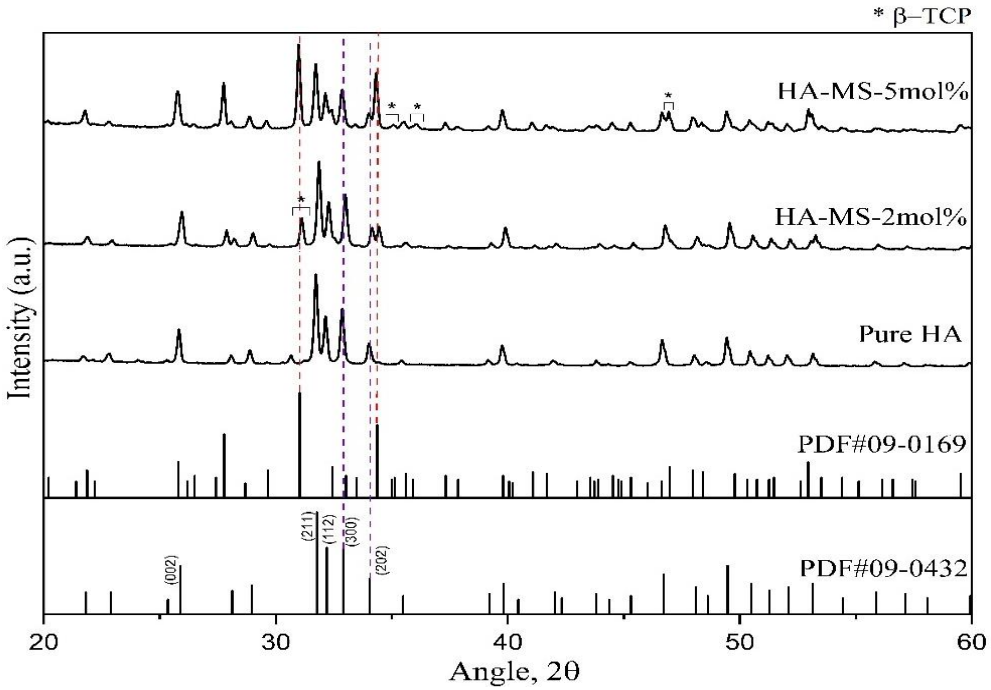

Figure 3.2. XRD patterns of Manganese-doped (manganese sulfate (MS) powder) HA samples sintered at 900 °C with two different concentrations. Vertical lines indicate the peaks of standard HA (PDF#09-0432), and β-TCP (PDF#09-0169).

Table 3.3. Phase amounts in HA and Mn-doped HA samples (with $MnSO_4$ precursor at 2 mol% and 5 mol% concentrations)

Sample	Phase Percentage (%)	
	900°C	
	HA	β-TCP
HA	99.80	0.20
Mn-HA ($MnSO_4$, 2 mol%)	75.30	24.70
Mn-HA ($MnSO_4$, 5 mol%)	45.90	54.10

Table 3.4. Calculation of degree of crystallinity of HA and Mn-doped HA samples (with $MnSO_4$ precursor at 2 mol% and 5 mol% concentrations)

Samples	Degree of Crystallinity (%)
	900°C
HA	85.87
Mn-HA ($MnSO_4$, 2 mol%)	90.06
Mn-HA ($MnSO_4$, 5 mol%)	92.23

3.1.1.2 Scanning Electron Microscopy (SEM)

In order to determine the morphology and size of the synthesized HA and Mn-HA, SEM analysis were applied to powders. Figure 3.3 shows the SEM images of the HA and Mn-HAs (with Manganese sulfate and Manganese chloride precursors) sintered at 900°C. The general shape was similar for all groups. With Mn involving groups, particles seemed to have more fusion forming irregular structures rather than spherical form in HA particles. Average particle size of the HA and Mn-HA powders were obtained by measuring with ImageJ software (National Institutes of Health, USA), and the resulting data were presented in Table 3.5. Average particle size of pure HA was found to be 139 nm, as reported in a previous study (Yedekçi et al., 2022). Average particle size of Mn-HA with manganese sulfate and manganese chloride as the precursors were 154 nm and 159 nm, respectively. Thus, there was no significant difference between the average particle sizes of Mn-doped HA groups with different sources of Mn. However, average particle size of HA increased with doping by Mn.

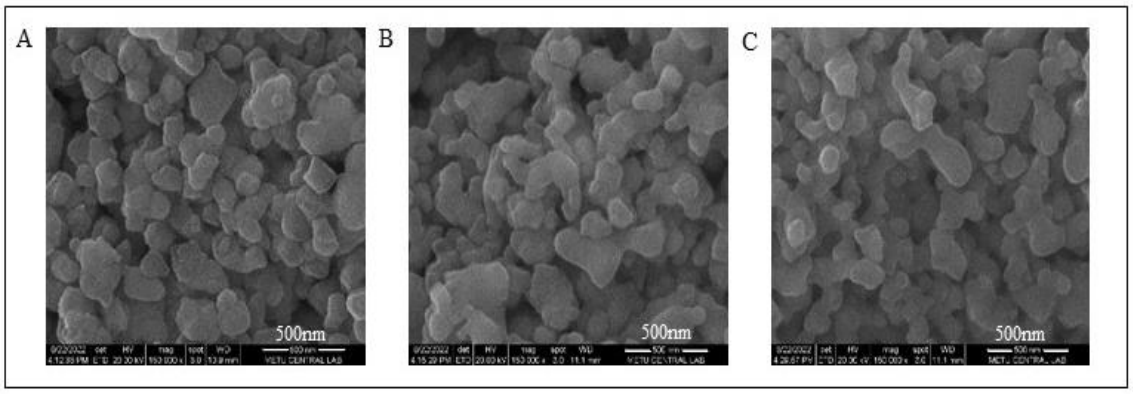

Figure 3.3. SEM graphs of HA and Mn-doped HA particles sintered at 900°C; A) Pure HA sample, B) Mn-HA sample (Manganese sulfate), C) Mn-HA sample (Manganese chloride) (Magnification: 150000X).

Table 3.5. The average particle size of HA and Mn-HA particles (with Manganese sulfate and Manganese chloride precursors) sintered at 900°C; A) Pure HA sample, B) Mn-HA sample (Manganese sulfate), C) Mn-HA sample (Manganese chloride)

Sample	Average Particle Size (nm)
Pure HA	139 ± 29.54
Mn-HA (Manganese sulfate)	154 ± 31.94
Mn-HA (Manganese chloride)	159 ± 43.22

3.1.1.3 Fourier Transform Infrared Spectroscopy (FTIR)

FTIR analysis was done to identify Figure 3.4 shows the FTIR spectra of the HA and Mn-HA (with Manganese sulfate and Manganese chloride precursors) samples collected at 4000-400 cm^{-1} region which are sintered at 800, 900, and 1000°C for 2h.

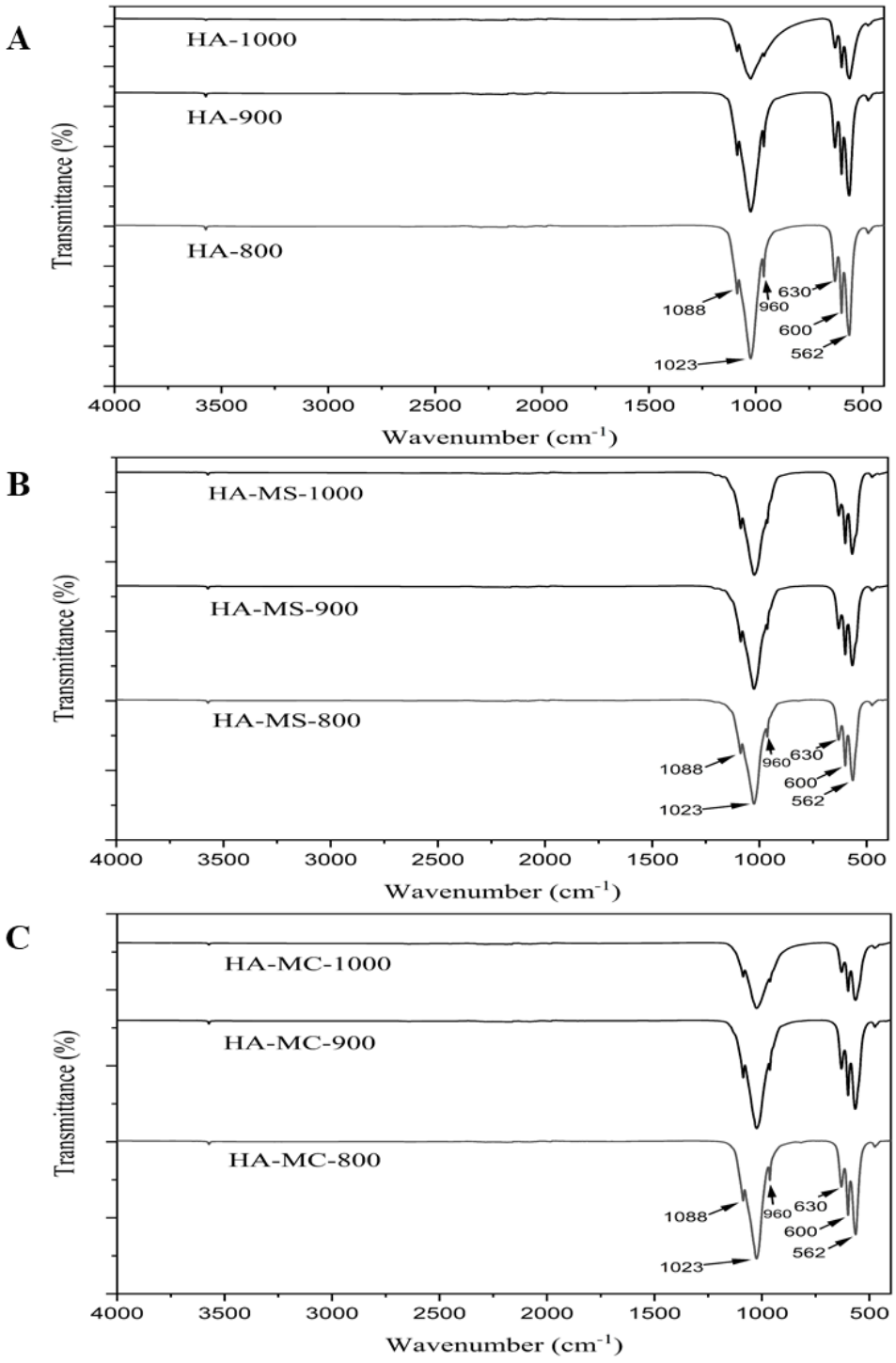

Figure 3.4. FTIR spectra of HA and Mn-HA sintered at 800, 900, and 1000°C; A) Pure HA sample, B) Mn-HA sample (Manganese sulfate (MS)), C) Mn-HA sample (Manganese chloride (MC))

According to FTIR spectra presented in Figure 3.4, all groups showed weak stretching band at 3573 cm^{-1} which is caused by the OH^- stretching mode of the HA phase. Vibration modes of PO_4^{3-} group were visible at 474 cm^{-1} (υ_2 P-O-P out of plane bending mode), 562 cm^{-1} and 600 cm^{-1} (υ_4 P-O-P in-plane bending mode), and 960 cm^{-1} (υ_1 P-O symmetric stretching mode), 1023 cm^{-1} and 1088 cm^{-1} (υ_3 P-O asymmetric stretching mode) (Kaya et al., 2021). PO_4^{3-} group related bands are the characteristics of the molecular structure of the polyhedrons of phosphate in apatite lattice (Paz et al., 2012). Bending modes of the band seen at 630 cm^{-1} were also attributed to the presence of the OH^- group in the HA phase. The bands related to the OH^- groups are the indication of bound water by weakening the strength of the bond between calcium and its hydration sphere in order to accelerate the de-aquation step and form apatite in aqueous solutions (Demirtaş et al., 2015). As seen in other studies, no band contributed to the presence of carbonate (CO_3^{2-}) groups between the 1380-1550 cm^{-1} range in Figure 3.4 (Kaya et al., 2021; Natasha et al., 2008).

Figure 3.5 shows the FTIR spectra of pure HA and Mn-HA (Manganese sulfate) with two different doping ratios (i.e., 2% and 5% (mol%) dopant). In Figure 3.5, OH^- absorption band decreases from pure HA to 2% Mn-HA; it vanishes as the percentage of doping element (Mn) increases to 5%. Disappearance of the OH^- band results in a spectrum that is characteristic of β-TCP. Additionally, this study shows that as Mn mol% in HA increases, PO_4^{3-} bands at 1024 cm^{-1} and 1087 cm^{-1} become sharper and narrower, as seen in Figure 3.5 (Natasha et al., 2008). Sharpening of the PO_4^{3-} bands at 1024-1087 cm^{-1} indicates an increase in the crystallinity of the Mn-doped samples. This result is in good accordance with XRD data confirming an increase in crystallinity as the Mn concentration increases. Moreover, with addition of 2% (mol) and 5% (mol) Mn as doping element, the υ_4 O-P-O bending band of HA at 601 cm^{-1} (Reid et al., 2006) and β-TCP at 594 cm^{-1} (Reid et al., 2006) tend to decrease (Natasha et al., 2008). No band related to the NH_4^+ ions at 875 cm^{-1} was observed which shows no residuals exists in the as-synthesized HA powders (Raynaud et al., 2002). In Figure 3.5, the bands at 600 cm^{-1} and 547 cm^{-1} in the 5% Mn-HA sample (Mn-MS-5mol%) are possibly the indication of β-TCP phase in the

structure of HA, as confirmed in previous studies (Moreira et al., 2016; Xidaki et al., 2018).

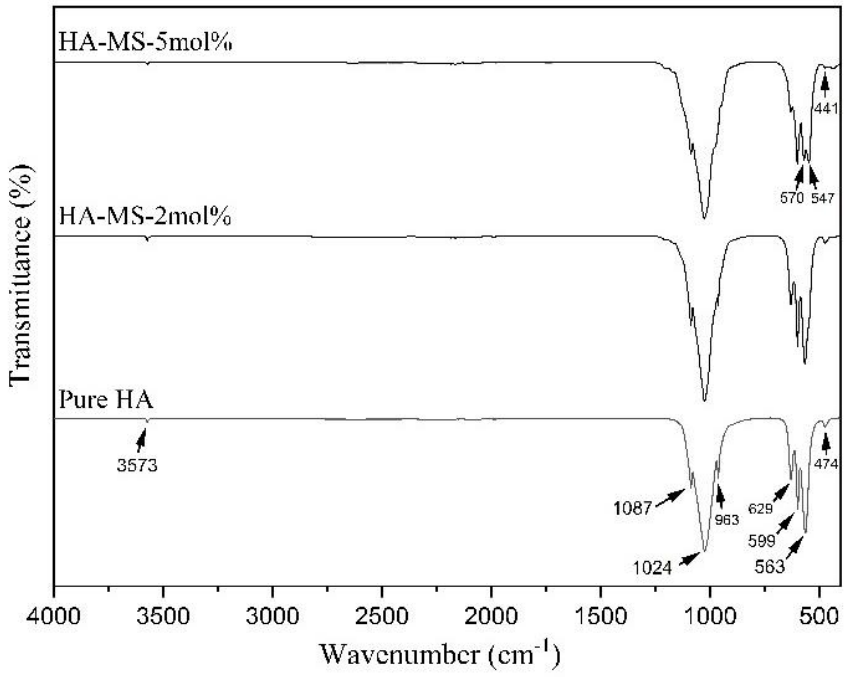

Figure 3.5. FTIR spectra of HA and Mn-HA (from manganese sulfate (MS) precursor) sintered at 900°C with 2% and 5% (mol%) doping concentrations; A) Pure HA sample, B) Mn-HA sample (2% Mn concentration), C) Mn-HA sample (5% Mn concentration)

3.1.1.4 Inductively Coupled Plasma-Mass Spectrometry (ICP-MS)

In order to verify the correctness of mol percent of Mn doped groups after dopping, ICP-MS analysis were applied. The chemical composition of HA and Mn-doped HA (from two different precursors, $MnSO_4$ and $MnCl_2$) were obtained by ICP-MS analysis and presented in Table 3.6. Accordingly, it can be suggested that Mn doping was successfull and the amount of Mn was in agreement with the theoretical values for both groups obtained by $MnSO_4$ and $MnCl_2$ powder sources.

Table 3.6. Chemical composition of HA and Mn-doped HA sintered at 900°C with two different precursors ($MnSO_4$ and $MnCl_2$) obtained with ICP-MS

Sample ID (mol)	***Ca***	***P***	***Mn***
Theoretical values	*1.00*	*0.60*	*0.02*
HA	0.90	0.58	0
(2%) HA-MS ($MnSO_4$*)*	0.87	0.57	0.02
(2%) HA-MC ($MnCl_2$*)*	0.87	0.57	0.02

The results of ICP-MS analysis revealed the presence of Mn in the Mn-HA samples. The data in Table 3.7 indicates that the measured values of Ca/P ratio are slightly lower than their theoretical values. This suggests that impurities like carbonates or acidic phosphates in the crystal core are causing the formation of a calcium-deficient form of HA instead of the ideal stoichiometric HA. Similarly, the ratio of (Ca + Mn)/P in the Mn-doped samples also indicates the calcium-deficient form of HA. The calcium-deficient HA would be more desirable as they are structurally similar to the natural bone. The comparison of theoretical and measured values of the Mn/Ca ratio shows that 2 mol% of Mn is properly substituted with Ca in HA structure.

Table 3.7. Theoretical and experimental composition of HA and Mn-doped HA sintered at 900°C with two different precursors ($MnSO_4$ and $MnCl_2$) in terms of their molar ratio.

Sample	***Theoretical molar ratio***			***Measured Molar ratio by ICP-MS***		
	Ca/P	(Ca+Mn)/P	Mn/Ca	Ca/P	(Ca+Mn)/P	Mn/Ca
HA	1.67	1.67	0	1.5457	1.5457	0
HA-Mn ($MnSO_4$*)*	1.63	1.67	0.02	1.5457	1.5827	0.0239
HA-Mn ($MnCl_2$*)*	1.63	1.67	0.02	1.5196	1.5566	0.0244

3.1.2 Scaffold Characterizations

3.1.2.1 SEM analysis of PCL, PCL/HA, and PCL/Mn-HA Scaffolds

The fibrous structure and fiber sizes of the formed scaffolds were examined by SEM analysis. Initially different concentrations of PCL were electrospun with or without HA or Mn-HA incorporation to determine best fibrous scaffold production conditions with these materials.

Morphologies of electrospun PCL scaffolds prepared with different concentrations (10%, 15%, 16% (w/v) of PCL concentration) are shown in Figures 3.6, 3.7, and 3.8. Accordingly, at lower concentrations of PCL (Fig. 16A-B, 10% PCL) the fibers had bulk, bead-like regions in presence or absence of Mn-HA which suggested that this concentration is not suitable for scaffold production.

As the PCL concentration increased, the beading of the fibers decreased, and the fiber thickness increased (Figure 3.7A-B, and Figure 3.8A-B). Bead-like structures in electrospun fibers are considered as defects and they can affect the fiber uniformity and diameter. In order to decrease the beading, different factors, such as voltage, polymer concentration, needle to collector distance, etc. can be optimized (Arrieta et al., 2020; Meireles et al., 2018). Thus, by comparing the samples in Figures 3.6, 3.7, and 3.8, 15% PCL scaffold shows the least beading and proper fiber thickness which can be used for further analysis.

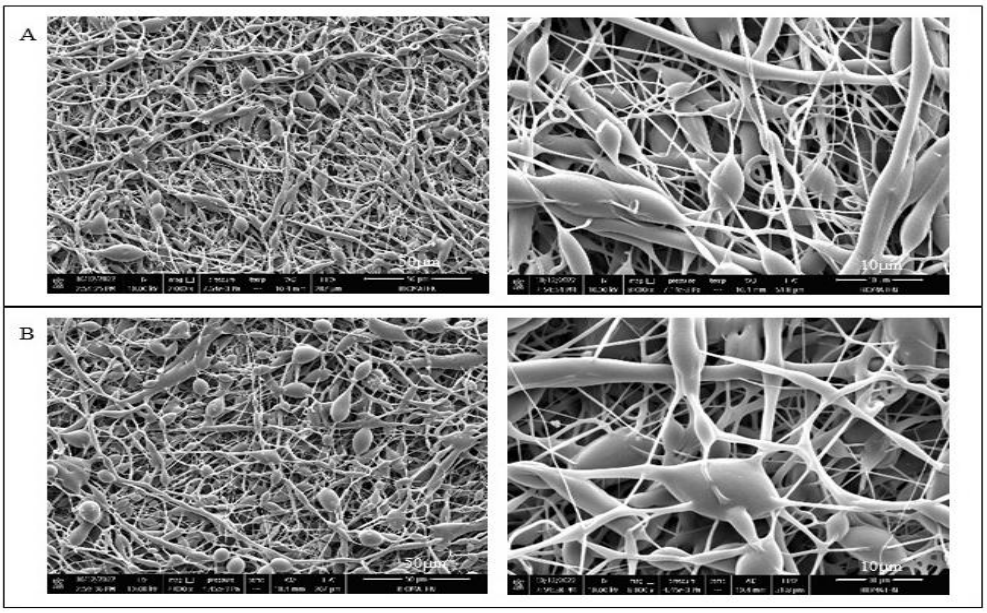

Figure 3.6. SEM analysis of the electrospun PCL scaffolds with different concentrations; A) 10% PCL, B) 10%PCL+5%Mn-HA scaffolds (Magnifications: 2000X (left column), 8000X (right column)).

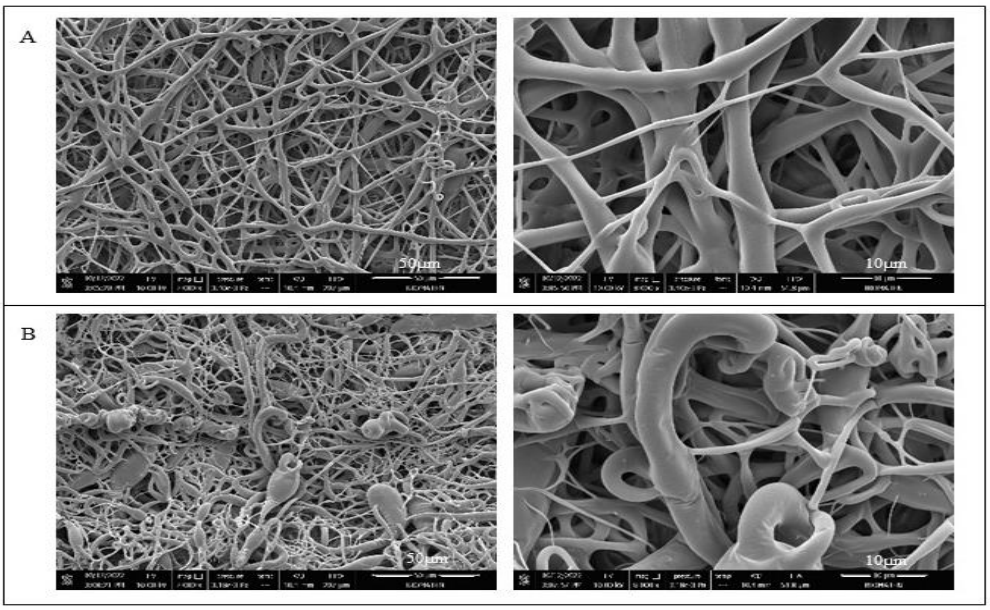

Figure 3.7. SEM analysis of the electrospun PCL scaffolds with different concentrations; A) 15%PCL, B) 15%PCL+5%Mn-HA scaffolds (Magnifications: 2000X (left column), 8000X (right column)).

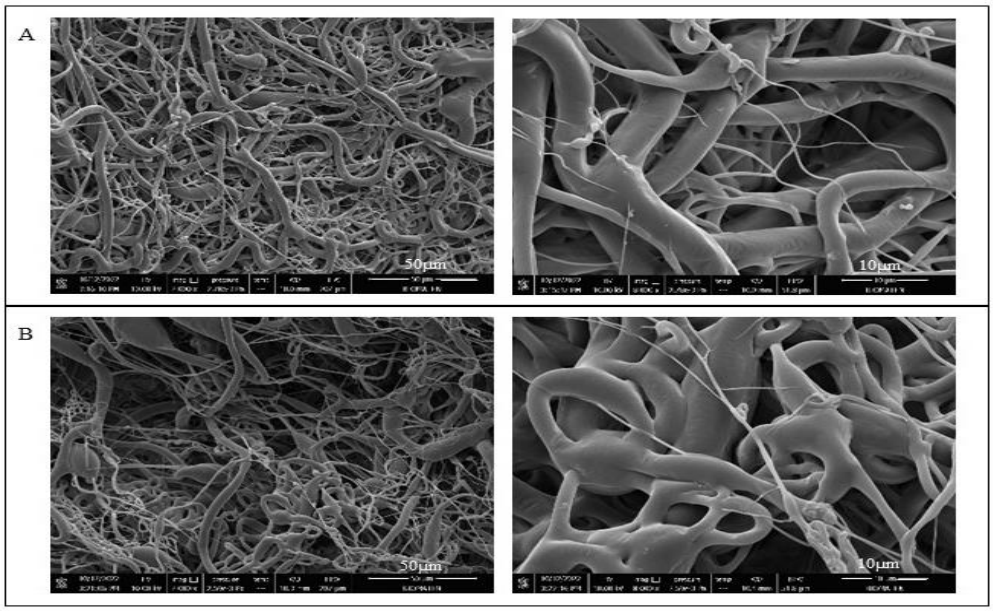

Figure 3.8. SEM analysis of the electrospun PCL scaffolds with different concentrations; A) 16%PCL, B)16%PCL+5%Mn-HA scaffolds (Magnifications: 2000X (left column), 8000X (right column)).

3.1.2.2 SEM Analysis of Gelatin-coated PCL, PCL/HA, and PCL/Mn-HA Scaffolds

In order to improve the biological properties of the fibrous PCL-HA scaffolds, they were coated with a thin layer of gelatin and crosslinked. SEM analysis of gelatin coated scaffolds showed that fibrous structure of the scaffolds was covered by the coated material. Coating was formed as small patches with boundaries probably due to the cross-linking agent (glutaraldehyde) that developed membranous regions at small areas until they contact with each other (Figure 3.9). Although surface of the scaffolds was mostly covered, the porous structure and the depth of the pores could also be observed in Figure 3.9-B by cross-section views of gelatin-coated PCL scaffold. In similar studies with gelatin coating strategy, the morphology of the gelatin-coating and its pore structure were observed to be in agreement with these SEM analyses (Lien et al., 2008, 2009).

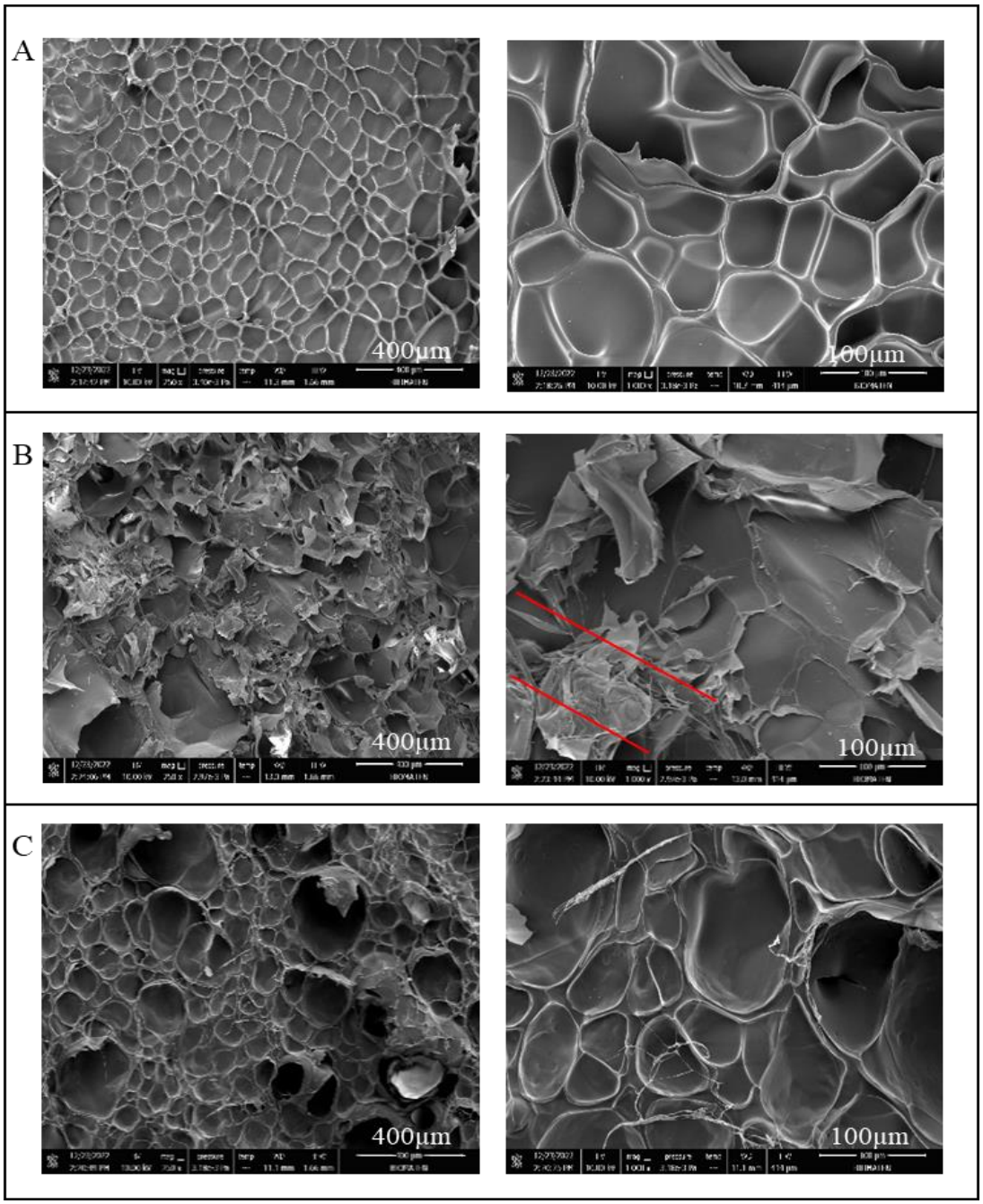

Figure 3.9. SEM analysis of the electrospun PCL scaffolds coated with gelatin; A) 15% PCL/gelatin (surface view), B) 15%PCL+2.5%Mn-HA (cross-section view), C) 15%PCL/gelatin+5%Mn-HA (surface view) scaffolds (Magnifications: 250X (left column), 1000X (right column)).

3.1.2.3 *In-Vitro* Degradation and Water Uptake Results

Different factors can affect the degradation of the polymers such as molecular structure, molecular weight, polymer composition, and the presence of cross-links, etc. (Göpferich, 1996).

As shown in Figure 3.10, a high amount of weight loss occurred in all groups at early time points, starting at day 1. Considering the well-known slow degradation profile of PCL and bioceramics, this early and high amount of degradation was thought to be related with gelatin. Hence, gelatin contributed to weight loss as the main factor during this period.

As seen in Figure 3.10, the 5% HA incorporated scaffold group showed the highest weight loss which is around 40% up to day 21. It was followed by the 15% PCL+2.5% HA scaffold which had about 30% weight loss at the end of 3rd week. Only PCL/gelatin scaffold and Mn-doped HA groups had relatively less weight loss, with 2.5% Mn-HA involving scaffolds being the one with least degradation profile.

The scaffold group with 5%Mn-HA had slightly higher weight loss than the that of 2.5% Mn-HA.

Therefore, as HA amount in scaffold increased, a considerable increase occurred in weight loss. Although the difference between two Mn-HA involving groups was very small, increase in Mn-HA concentration again increased the weight loss. By comparing groups containing HA with Mn-HA, it can be indicated that in Mn-HA involving groups degradations were less than HA incorporated ones.

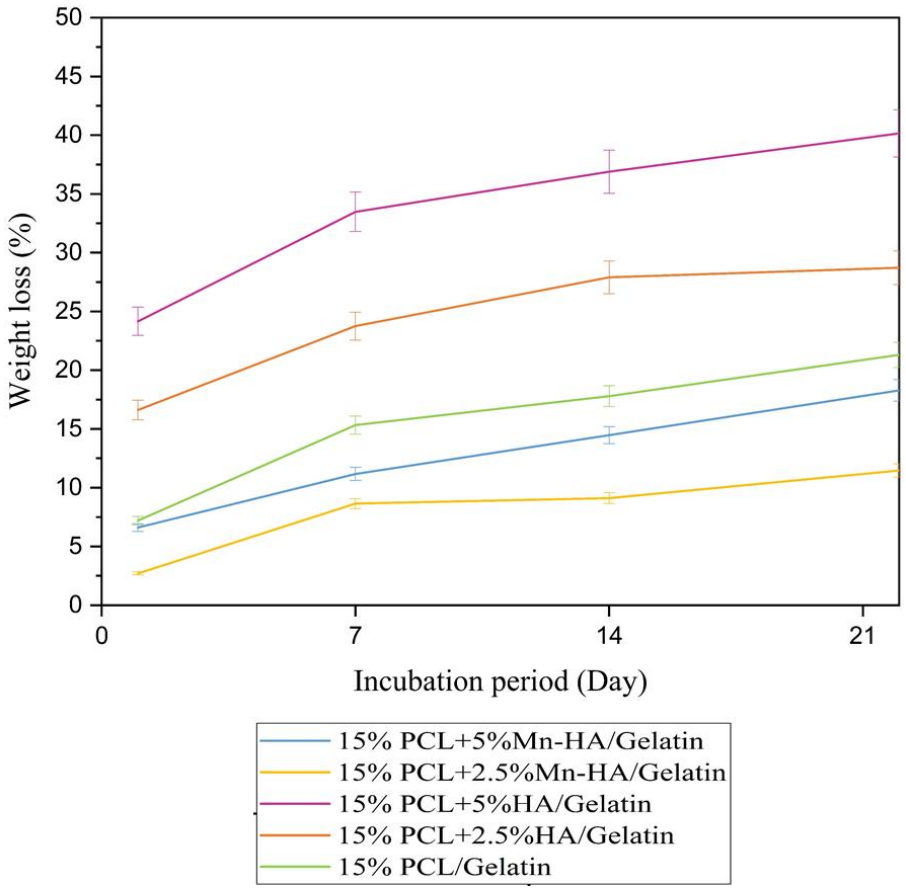

Figure 3.10. Weight loss (%) of the gelatin-coated sscaffolds (n=3).

The water uptake indicates the capacity of the scaffolds to transport and exchange proteins and other soluble substances with the surrounding environment, which can also promote cellular invasion (Long et al., 2015).

The water uptake experiments of scaffolds showed an increase pattern from day 1 to day 14 (Figure 3.11). Since the degradation started very early in all groups, the water uptake was not expected to have this increase profile; however, due to the thickness of gelatin-coated layer (5-6mm overall thickness of scaffolds) it shows an increasing pattern up to day 14 after which it declines.

Besides the effect of hydrophilic components in water uptake property of scaffolds, fibrous nature of electrospun scaffolds that involves 3-D porous architecture inside

is also known to be a cause for high water uptake. Based on a study done by Pattanashetti et al. (2020), a noticeable degradation was observed after the addition of HA into PCL scaffold, on day 5 of incubation in PBS; this indicates that the incorporation of HA into PCL scaffold structure increases the rate of scaffold's degradation (Pattanashetti et al., 2020)

However, there was no conclusive difference in water uptake profiles between groups in accordance with presence of HA or Mn-HA and their ratios to PCL.

Although water uptake values were quite high even on the 1st day, no significant change in scaffold shape or structure (like swelling) was observed.

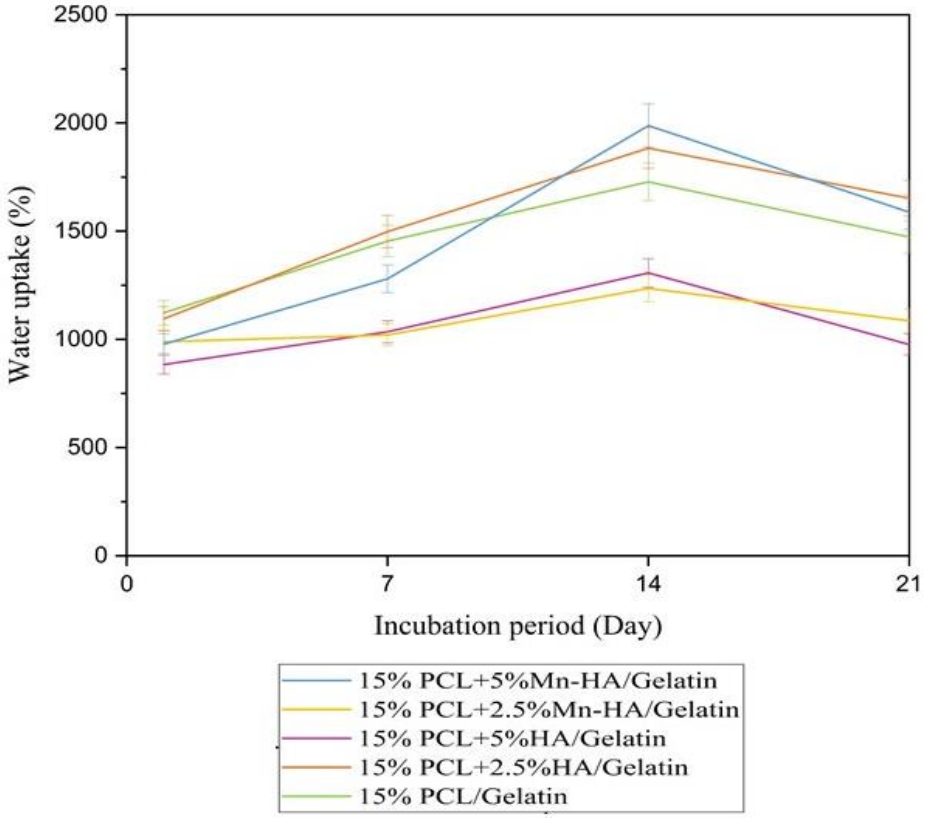

Figure 3.11. Water uptake (%) of the gelatin-coated samples (n=3).

3.1.2.4 *In-Vitro* Bioactivity Results

The bioactivity analysis was done for evaluation of the potency of the scaffolds for mineral accumulation or formation on their surfaces. As seen in Figure 3.12, the SEM images for day 7 incubation results of scaffolds showed that all groups have CaP involving (apatite-like) particles formed on their surfaces. The CaP particles can be seen in various shapes. The EDX analysis also confirmed the presence of calcium (Ca) and phosphate (P) elements in the apatite-like structures (as seen in Table 3.8).

Table 3.8. Calculation of Ca/P ratio of gelatin-coated scaffolds from EDX data

SAMPLES	Ca/P ratio	
	Day 7	Day 14
15%PCL/gelatin	2.14	1.56
15%PCL + 2.5%HA/gelatin	1.72	1.69
15%PCL + 5%HA/gelatin	1.71	1.70
15%PCL + 2.5%Mn-HA/gelatin	1.86	1.75
15%PCL + 5%Mn-HA/gelatin	1.50	1.30

Similarly, in Figure 3.13, the SEM images revealed mineral formations on most scaffold surfaces upon day 14 of incubation in SBF. It can be seen that in all groups, except Figure 3.13-C (15% PCL + 5% HA) CaP (apatite like) formations were more than day 7 results. The EDX showed that the particles formed on the surface of PCL+5%HA contain Na, Cl, C, and K elements in their structure. The same particle structure seen in Figure 3.13-C can be also observed in Figure 3.12-B; the EDX confirmed the presence of CaP precipitates in the chemical structure of these particles.

Figures 3.12 and 3.13 show the gradual increase in the amount of apatite formation from day 7 to 14. The Ca and P (wt%) values from EDX data can be used to calculate the Ca/P ratio. Based on the EDX results, the Ca/P ratio for samples at day 7 and 14 ranges from 1.30-2.14 which is close to stoichiometric value of Ca/P ratio (1.67) in HA in bone. This shows that the accumulated CaP formed is similar to the biological apatite in body.

The bioactivity test was performed to confirm that the material has the ability to bond to living bone; so, when the material is implanted in the body, it has to be able to create bone-like apatite on its surface. SBF can mimic the bone environment in terms of similarity in ion concentrations. Therefore, the scaffold can be placed in SBF to see whether the apatite layer forms on its surface. The capability of the scaffold to form an apatite layer indicates that the material can form interfacial bonds with surrounding bone tissues when they are placed in physiological environment (Jose & Alagar, 2015; Kokubo & Takadama, 2006).

In a study by Bigi et al (2002), the deposition of the apatite occurred on the borders of the gelatin pores, and the shape of the presented CaP particles were similar to the spherical precipitates seen in this thesis (Bigi et al., 2002). Also, this study confirms the Ca/P ratio of CaP particles being in 1.40-1.60 range which is again the biological Ca/P range (Bigi et al., 2002).

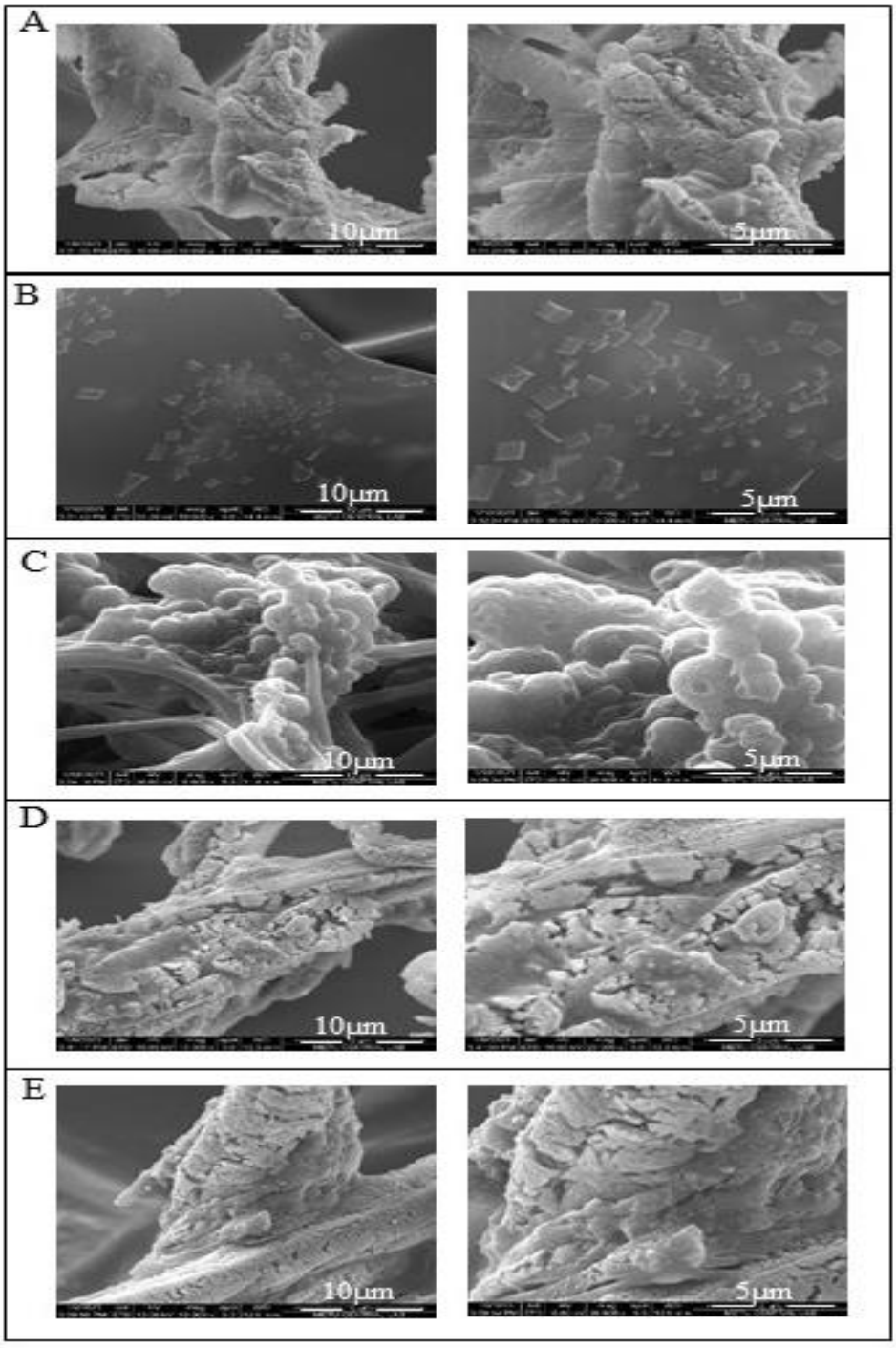

Figure 3.12. Apatite formation (Ca and P accumulation) on PCL/gelatin/HA and PCL/gelatin/Mn-HA scaffolds on day 7 of incubation in SBF at 37°C; A) 15% PCL. scaffold, B) 15%PCL + 2.5%HA, C) 15%PCL + 5%HA, D) 15%PCL + 2.5%Mn-HA, E) 15%PCL + 5%Mn-HA scaffolds (Magnifications: 10000X (left column), 20000X (right column)).

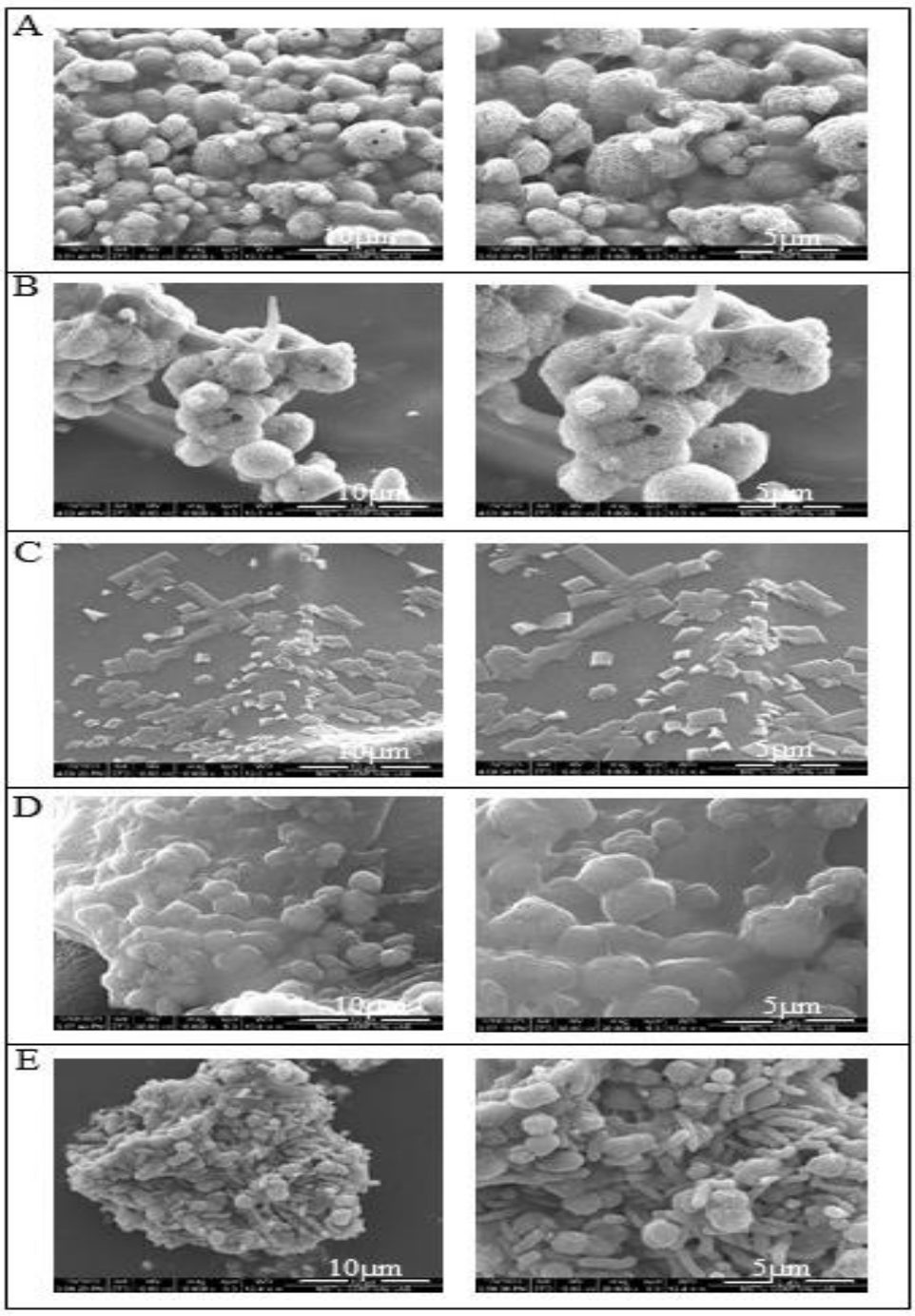

Figure 3.13. Apatite formation (Ca and P accumulation) on PCL/gelatin/HA and PCL/gelatin/Mn-HA scaffolds on day 14 of incubation in SBF at 37°C; A) 15% PCL scaffold, B) 15%PCL + 2.5%HA, C) 15%PCL + 5%HA, D) 15%PCL + 2.5%Mn-HA, E) 15%PCL + 5%Mn-HA scaffolds (Magnifications: 10000X (left column), 20000X (right column)).

During the bioactivity test, the pH of the SBF solutions was measured every 2 days. According to Figure 3.14, the pH changes were comparable for all groups and pH values were measured to be between 7.34-7.55 which is in biological range. Therefore, none of the scaffolds show any sudden ion release which can result in significant pH change and adverse effects on the cells. As seen in Figure 3.14, there was a small increase in pH in the first 2 days; this could be because of the exchange of the H^+ ion of SBF with the Ca^{2+} ions on the scaffolds' surface (Gu et al., 2004).

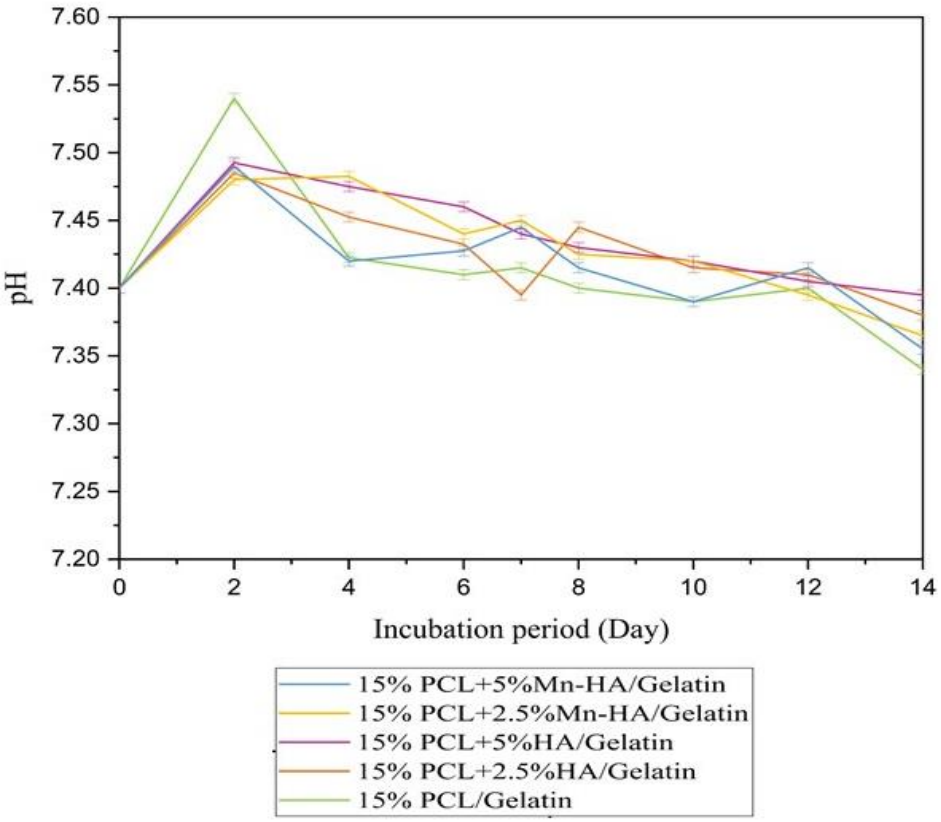

Figure 3.14. Changes in pH of SBF during bioactivity tests of scaffolds (n=2)

3.1.3 Biological Characterization of Synthesized HA/Mn-HA Particles and Scaffolds

3.1.3.1 Cell Culture Analyses

3.1.3.1.1 Indirect Cytotoxicity Test of HA and Mn-HA Powders

In order to evaluate the effect of Mn on cell viability, the L-929 fibroblast cells were used for indirect cytotoxicity test. Pure HA and Mn-doped HAs with two different precursors (manganese sulfate and manganese chloride) were used in the indirect cytotoxicity tests to see if there is any toxic effect related with extract concentrations or composition (or precursors) of the synthesized HA and Mn-doped HA particle. Cells grown on culture plate without any extract addition were used as control.

The powder extractions were done for testing the effect of synthesized particles on cells' viability. The doubling time of L-929 is less than 48 h (Bucur et al., 2019), thus, the Alamar blue test was performed on days 1 and 2 after addition of extracts. After extraction of the particles with incubation in cell growth medium, they were diluted (with the same medium at different dilution ratios) at different ratios.

According to Figure 3.15, Mn-HA ($MnSO_4$ source) showed a better effect on cell viability both on days 1 and 2. The Mn-HA ($MnSO_4$ source) extracts at 1x and 1/4x amounts showed the highest viability percentage. The Mn-HA ($MnCl_2$ source) also showed good viability at 1x and 1/2x amounts on day 1. All groups of extracts were comparable for day 2 except Mn-HA ($MnCl_2$ source) ones. The overall result indicated that the Mn-HA ($MnSO_4$ source) has better cell viability than Mn-HA ($MnCl_2$ source). This might be related to the introduction of some minute amounts of chloride element from this source during bioceramics synthesis steps. Thus, Mn-HA ($MnSO_4$ source) was considered as a more appropriate choice to be used in combination with PCL/gelatin scaffold for further analysis.

Previous studies showed that the biocompatibility and positive effect of HA on proliferation of the cells (Lee et al., 2013; Zhang et al., 2015). However, here, it was found that at lower dilutions (1x, 1/2x) HA extracts provided less viability than control and higher dilutions of this group, for both time points.

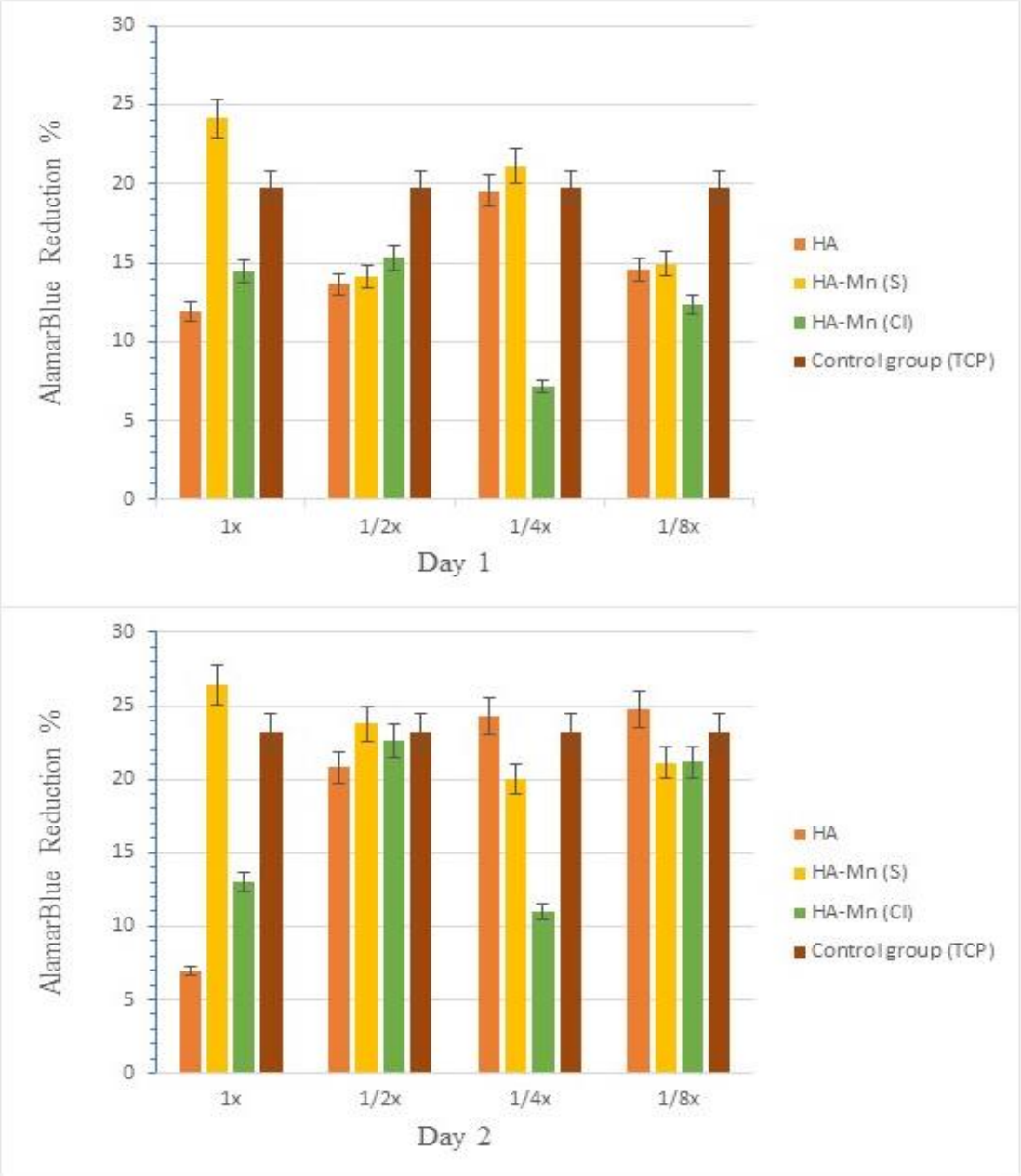

Figure 3.15. Indirect cytotoxicity test for HA and Mn-HA (with Mn-sulfate (HA-Mn(S)) and Mn-chloride (HA-Mn(Cl)) precursors) on day 1 and day 2 (n=5).

3.1.3.1.2 Cell Viability on of PCL/Gelatin scaffolds incorporated with HA and Mn-HA

The effect of Mn-doping of HA, amount of HA/Mn-HA in scaffolds and gelatin coating on cell viability characteristics of scaffolds were analyzed with cell viability test using Saos-2 cells (human osteosarcoma cell line). Here, viability of cells seeded on scaffolds were followed for 1, 4 and 7 days to evaluate attachment and proliferation potencies of the scaffolds besides their cytocompatibility property. In this test, 15% PCL group (without gelatin coating) was also added to the study to see the effect gelatin coating on the cells' viability. Cells seeded on cell culture plate were used as the control for all groups (TCP) and viabilities were calculated relative to this group. As seen in Figure 3.16, all gelatin-coated groups had positive effect on cell viability since the viability percentage of these groups were higher than the uncoated and TCP groups at all time points.

The relative viability values of coated scaffold groups increased in general from day 1 to day 4. However, the relative viability of all coated scaffold groups was similar from day 4 to day 7, which might be related with cells reaching confluency and/or passing into a more differentiated stage with increased osteogenic activities following proliferation. Only 15%PCL/gelatin+5%HA showed a different pattern; the increase in relative viability for this group was also recognizable at day 7. This shows that other than gelatin, the concentration of HA might have a positive effect on cell viability. No significant difference has been observed between the different concentrations of HA and Mn-doped HA samples. For Mn-HA containing groups, the viability (%) increased slightly when the concentration of Mn-doped HA increased, and this pattern can be seen in all three incubation periods. By comparing gelatin-coated groups with the TCP group, no toxic effect can be seen, as the relative cell viability (%) is higher for all gelatin-coated groups compared to TCP group. However, 15%PCL group (without gelatin) showed less cell viability which was an

unexpected outcome considering PCL related literature. Thus, it was thought that this might be due to some initial less seeding or attachment efficiency of the cells in this scaffold group. Overall results suggest that the PCL/gelatin scaffolds containing 5% HA and 5 % Mn-HA can be considered as more suitable groups in terms of their effect on cell viability properties.

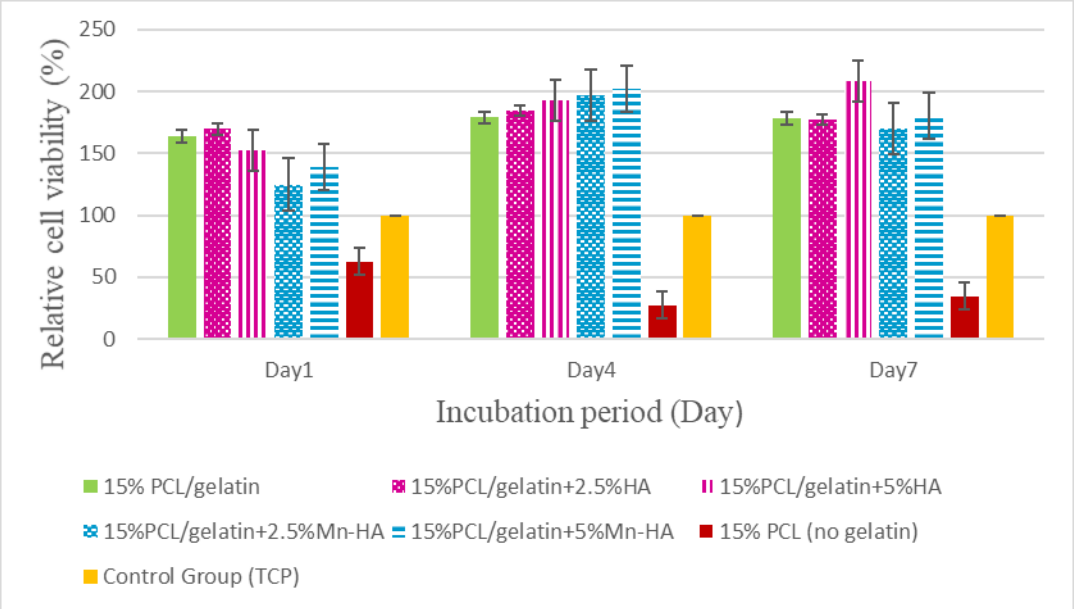

Figure 3.16. Cell viability results on gelatin-coated samples (at day 1, 4, and 7).

In previous studies, it was confirmed that the Mn-doped HA has osteogenic effect, and it improves the spread of the osteoblast cells on the surface of the material containing Mn-doped HA (Bigi et al., 2005; Paluszkiewicz et al., 2010).

The SEM results of the Saos-2 cells grown on scaffolds showed that all the gelatin coated groups had very thick coat-like covering on their surfaces at day 7 (Figure 3.17). However, it was difficult to indicate cells exactly on images. Therefore, surface of coated scaffolds with or without cells were compared as seen in Figure 3.18. Accordingly, it was thought that cells might have spread on the gelatin surface forming a different surface morphology.

Unlike these groups, pure PCL scaffold (without gelatin coating) (Figure 3.17-F) did not have any such layers on its surface upon cell culture incubation. Thus, it might be related with either absence of gelatin coat and/or due to the improper attachment of the cells to this scaffold group.

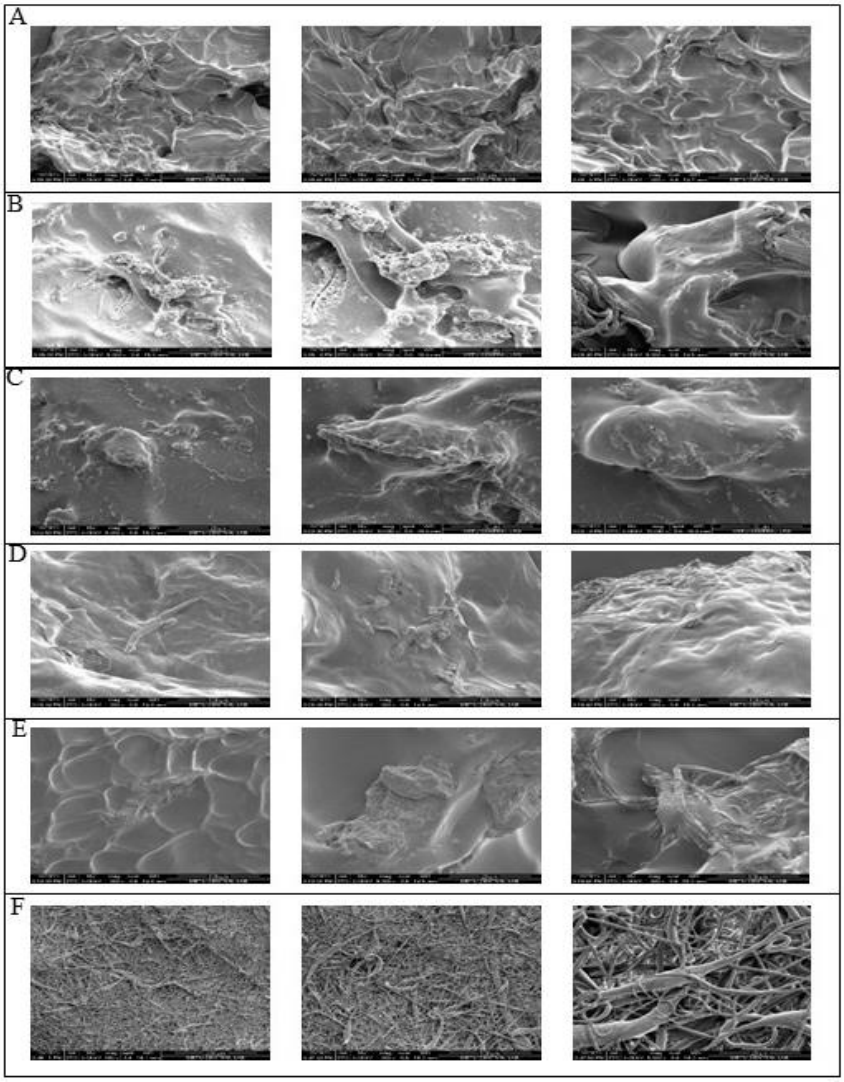

Figure 3.17. SEM images of the PCL and gelatin-coated PCL-HA, PCL-MnHA Scaffolds, after 7 incubation (n=5); A) 15% PCL scaffold with gelatin coating, B) 15%PCL + 2.5%HA, C) 15%PCL + 5%HA, D) 15%PCL + 2.5%Mn-HA, E) 15%PCL + 5%Mn-HA, F) 15%PCL (uncoated) scaffolds (Magnifications: 5000X (left column), 10000X (right column)).

Based on the Figure 3.18, due to the different surface morphology between the scaffolds without cells (Figure 3.18, left figures), and with cells (Figure 3.18, right figures), it can be interpreted that the cells formed a layer on the surface of the scaffolds due to presence of gelatin. However, more experimental research like confocal microscopy analysis and/or different incubation condition experiments would be needed to make a final conclusion.

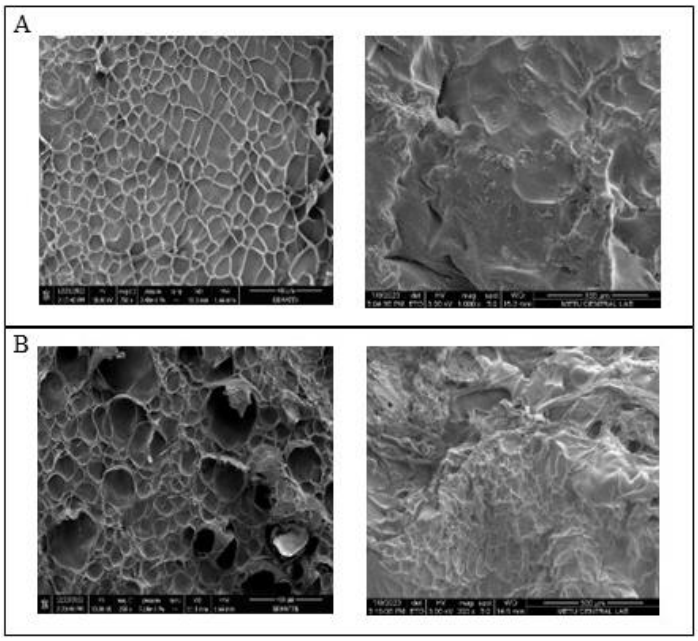

Figure 3.18. SEM images of the gelatin coated samples without and with cells; A)15%PCL/gelatin, B)15%PCL/gelatin+5%Mn-HA scaffolds (Magnification: 200X).

3.1.3.1.3 Osteogenic Activity of Cells

Osteogenic cell activity can be measured by ALP (alkaline phosphatase) which is a natural enzyme produced by osteoblasts during osteogenesis. The specific ALP activity of Saos-2 cells on gelatin coated PCL scaffolds can be seen in Figure 3.19. As seen in Figure 3.19, 5% concentration of HA and Mn-doped HA increased the ALP activity level, compared to 2.5% containing HA and Mn-doped HA groups on

both time points (day7 and 14), except for the Mn-doped HA group on day 7 which shows a decrease by increasing Mn-doped HA concentration. The Highest ALP activity can be observed in 5%HA group on day 7, and 5% Mn-doped HA group on day 14. Based on a previously reported study (Park et al., 2011), ALP activity of cells increased with time in PCL/HA scaffolds. The addition of HA affected positively in terms of cell proliferation and differentiation in PCL/HA scaffolds (Park et al., 2011). Additionally, in another study, it was presented that increase in HA concentration, increased ALP activity of cells in PCL containing HA scaffolds (Li et al., 2021, Shor et al., 2007).

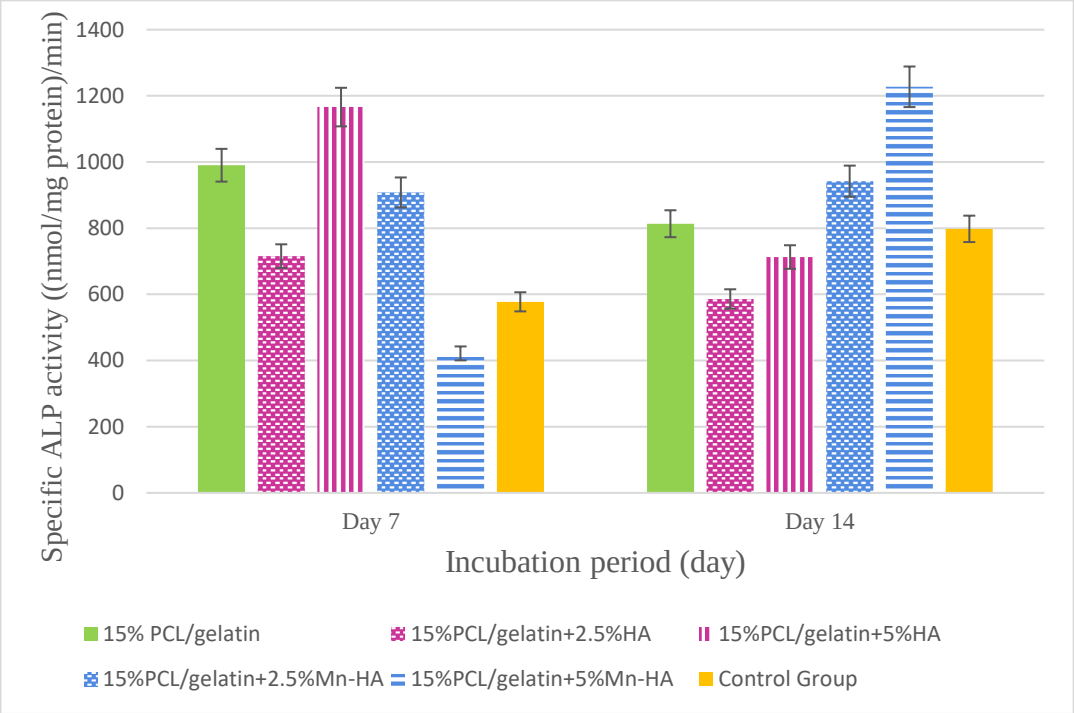

Figure 3.19. Specific ALP activity of Saos-2 cells on gelatin-coated samples (at day 7 and 14); control group is gelatin coated scaffold without cells.

CHAPTER 4

CONCLUSION

In this study, the effect of gelatin coating on PCL incorporated HA and Mn-doped HA was investigated. Based on structural analysis done by XRD and FTIR, the presence of manganese in hydroxyapatite structure was determined. The increase in sintering temperature increased the amount of biphasic structure in HA samples. The results showed that there was no significant difference between different groups of manganese-doped HA with different precursors and the samples with different sintering temperatures. The effect of cross-linked gelatin coating and incorporation of HA and Mn-doped HA on PCL scaffolds was investigated by *in vitro* degradation, bioactivity, indirect and direct cytotoxicity tests. The results showed that while HA increased degradation of gelatin coated PCL scaffolds, Mn doped HA has the opposite effect. Both HA and Mn-HA were very effective on improvement of mineralization of the scaffolds and there was no cytotoxic effect from Mn-doped HA powder extracts on L-929 cells. The presence of Mn-doped HA improved the water uptake ability of scaffolds bioactivity of the cells. The addition of a gelatin coat considerably increased viability of Saos-2 cells on scaffolds. Among these groups PCL/2.5% Mn-HA and PCL/5%HA groups showed slightly higher viability than the other groups. Overall, the results show that the addition of Mn-HA and gelatin to the primary PCL scaffold boosted the properties of scaffold which makes them a promising candidate for BTE applications.

REFERENCES

Alshemary, A. Z., Engin Pazarceviren, A., Tezcaner, A., & Evis, Z. (2018). Fe^{3+} /SeO_4^{2-} dual doped nano hydroxyapatite: A novel material for biomedical applications. *Journal of Biomedical Materials Research. Part B, Applied Biomaterials*, *106*(1), 340–352. https://doi.org/10.1002/JBM.B.33838

Alshemary, A. Z., Goh, Y. F., Akram, M., Razali, I. R., Abdul Kadir, M. R., & Hussain, R. (2013). Microwave assisted synthesis of nano sized sulphate doped hydroxyapatite. *Materials Research Bulletin*, *48*(6), 2106–2110. https://doi.org/10.1016/J.MATERRESBULL.2013.02.015

Amini, A. R., Laurencin, C. T., & Nukavarapu, S. P. (2012). Bone tissue engineering: Recent advances and challenges. *Critical Reviews in Biomedical Engineering*, *40*(5), 363. https://doi.org/10.1615/critrevbiomedeng.v40.i5.10

Arjunan, A., Baroutaji, A., Praveen, A. S., Robinson, J., & Wang, C. (2021). Classification of Biomaterial Functionality. *Encyclopedia of Smart Materials*, 86–102. https://doi.org/10.1016/B978-0-12-815732-9.00027-9

Arrieta, M. P., Gil, A. L., Yusef, M., Kenny, J. M., & Peponi, L. (2020). Electrospinning of PCL-based blends: Processing optimization for their scalable production. *Materials*, *13*(17), 3853. https://doi.org/10.3390/MA13173853

Bigi, A., Boanini, E., Panzavolta, S., Roveri, N., & Rubini, K. (2002). Bonelike apatite growth on hydroxyapatite–gelatin sponges from simulated body fluid. *Journal of Biomedical Materials Research*, *59*(4), 709–715. https://doi.org/10.1002/JBM.10045

Bigi, A., Bracci, B., Cuisinier, F., Elkaim, R., Fini, M., Mayer, I., Mihailescu, I. N., Socol, G., Sturba, L., & Torricelli, P. (2005). Human osteoblast response to pulsed laser deposited calcium phosphate coatings. *Biomaterials*, *26*(15), 2381–2389. https://doi.org/10.1016/J.BIOMATERIALS.2004.07.057

Boraschi-Diaz, I., Wang, J., Mort, J. S., & Komarova, S. V. (2017). Collagen type I as a ligand for receptor-mediated signaling. *Frontiers in Physics*, *5*, 12. https://doi.org/10.3389/FPHY.2017.00012

Boyce, B., Yao, Z., & Xing, L. (2009). Osteoclasts have multiple roles in bone in addition to bone resorption. *Critical Reviews in Eukaryotic Gene Expression*, *19*(3), 171-180. https://doi.org/10.1615/CRITREVEUKARGENEEXPR.V19.I3.10

Bracci, B., Torricelli, P., Panzavolta, S., Boanini, E., Giardino, R., & Bigi, A. (2009). Effect of Mg^{2+}, Sr^{2+}, and Mn^{2+} on the chemico-physical and in vitro biological properties of calcium phosphate biomimetic coatings. *Journal of Inorganic Biochemistry*, *103*(12), 1666–1674. https://doi.org/10.1016/J.JINORGBIO.2009.09.009

Breeland, G., Sinkler, M. A., & Menezes, R. G. (2022). Embryology, Bone Ossification. *StatPearls*. https://www.ncbi.nlm.nih.gov/books/NBK539718/

Bucur, M., Constantin, C., Neagu, M., Zurac, S., Dinca, O., Vladan, C., Cioplea, M., Popp, C., Nichita, L., & Ionescu, E. (2019). Alveolar blood clots and platelet-rich fibrin induce in vitro fibroblast proliferation and migration. *Experimental and Therapeutic Medicine*. 17(2), 982-989. https://doi.org/10.3892/ETM.2018.7063

Cacciotti, I. (2019). Multisubstituted hydroxyapatite powders and coatings: The influence of the codoping on the hydroxyapatite performances. *International Journal of Applied Ceramic Technology*, *16*(5), 1864–1884. https://doi.org/10.1111/IJAC.13229

Choi, M. O., & Kim, Y. J. (2012). Fabrication of gelatin/calcium phosphate composite nanofibrous membranes by biomimetic mineralization. *International Journal of Biological Macromolecules*, *50*(5), 1188–1194. https://doi.org/10.1016/J.IJBIOMAC.2012.04.001

Clarke, B. (2008). Normal bone anatomy and physiology. *Clinical Journal of the American Society of Nephrology*, *3*(Supplement 3), S131-S139. https://doi.org/10.2215/CJN.04151206

Demirtaş, T. T., Kaynak, G., & Gümüşderelioğlu, M. (2015). Bone-like hydroxyapatite precipitated from 10×SBF-like solution by microwave irradiation. *Materials Science and Engineering: C*, *49*, 713–719. https://doi.org/10.1016/J.MSEC.2015.01.057

Farzadi, A., Solati-Hashjin, M., Bakhshi, F., Aminian, A., (2011). Synthesis and characterization of hydroxyapatite/β-tricalcium phosphate nanocomposites using microwave irradiation. Ceram. Int. 37, 65–71. https://doi.org/10.1016/j.ceramint.2010.08.021

Feng, X. (2009). Chemical and biochemical basis of cell-bone matrix interaction in health and disease. *Current chemical biology*, *3*(2), 189-196. PMCID: PMC2790195

Fuh, L. J., Huang, Y. J., Chen, W. C., & Lin, D. J. (2017). Preparation of micro-porous bioceramic containing silicon-substituted hydroxyapatite and beta-tricalcium phosphate. *Materials Science and Engineering: C*, *75*, 798–806. https://doi.org/10.1016/J.MSEC.2017.02.065

Ghasemi-Mobarakeh, L., Kolahreez, D., Ramakrishna, S., & Williams, D. (2019). Key terminology in biomaterials and biocompatibility. *Current Opinion in Biomedical Engineering*, *10*, 45–50. https://doi.org/10.1016/J.COBME.2019.02.004

Ghayor, C., Chen, T. H., Bhattacharya, I., Özcan, M., & Weber, F. E. (2020). Microporosities in 3D-printed tricalcium-phosphate-based bone substitutes enhance osteoconduction and affect osteoclastic resorption. International Journal of Molecular Sciences, 21(23), 9270. https://doi.org/10.3390/ijms21239270

Göpferich, A. (1996). Mechanisms of polymer degradation and erosion. *Biomaterials*, *17*(2), 103–114. https://doi.org/10.1016/0142-9612(96)85755-3

Gu, Y. W., Khor, K. A., & Cheang, P. (2004). Bone-like apatite layer formation on hydroxyapatite prepared by spark plasma sintering (SPS). *Biomaterials*, *25*(18), 4127–4134. https://doi.org/10.1016/J.BIOMATERIALS.2003.11.030

Guo, L., Huang, M., & Zhang, X. (2003). Effects of sintering temperature on structure of hydroxyapatite studied with Rietveld method. *Journal of Materials Science: Materials in Medicine*, *14*, 817-822. https://doi.org/10.1023/A:1025048724330

Haider, A., Haider, S., & Kang, I. K. (2018). A comprehensive review summarizing the effect of electrospinning parameters and potential applications of nanofibers in biomedical and biotechnology. *Arabian Journal of Chemistry*, *11*(8), 1165–1188. https://doi.org/10.1016/J.ARABJC.2015.11.015

He, P., Sahoo, S., Ng, K. S., Chen, K., Toh, S. L., & Goh, J. C. H. (2013). Enhanced osteoinductivity and osteoconductivity through hydroxyapatite coating of silk-based tissue-engineered ligament scaffold. Journal of biomedical materials research part A, 101(2), 555-566. https://doi.org/10.1002/jbm.a.34333

Henao, J., Poblano-Salas, C., Monsalve, M., Corona-Castuera, J., & Barceinas-Sanchez, O. (2019). Bio-active glass coatings manufactured by thermal spray: A status report. *Journal of Materials Research and Technology*, *8*(5), 4965–4984. https://doi.org/10.1016/J.JMRT.2019.07.011

Hutmacher, D. W. (2000). Scaffolds in tissue engineering bone and cartilage. *Biomaterials*, *21*(24), 2529–2543. https://doi.org/10.1016/S0142-9612(00)00121-6

ISO, I. (2012). 10993–12: 2021 Biological evaluation of medical devices-Part 12: Sample preparation and reference materials. *International Organization for Standardization (ISO): Geneva, Switzerland*.

Jodati, H., Yilmaz, B., & Evis, Z. (2020). Calcium zirconium silicate (baghdadite) ceramic as a biomaterial. *Ceramics International*, *46*(14), 21902–21909. https://doi.org/10.1016/J.CERAMINT.2020.06.105

Jose, A. J., & Alagar, M. (2015). Preparation and characterization of polysulfone-based nanocomposites. *Manufacturing of Nanocomposites with Engineering Plastics*, Woodhead Publishing, 31–59. https://doi.org/10.1016/B978-1-78242-308-9.00003-3

Kang, J. I., Son, M. K., Choe, H. C., & Brantley, W. A. (2016). Bone-like apatite formation on manganese-hydroxyapatite coating formed on Ti-6Al-4V alloy by plasma electrolytic oxidation. *Thin Solid Films*, *620*, 126-131. https://doi.org/10.1016/j.tsf.2016.07.088

Kaya, Y., Jodati, H., & Evis, Z. (2021). Effects of biomimetic synthesis route and sintering temperature on physicochemical, microstructural, and mechanical properties of hydroxyapatite. *Journal of the Australian Ceramic Society*, *57*(4), 1117–1129. https://doi.org/10.1007/s41779-021-00609-x

Khurana, J. S., McCarthy, E. F., & Zhang, P. J. (2010). *Essentials in Bone and Soft-Tissue Pathology*, Springer. https://doi.org/10.1007/978-0-387-89845-2

Koksal, O. K., Apaydın, G., Tozar, A., Karahan, İ. H., & Cengiz, E. (2019). Assessment of the mass attenuation parameters with using gamma-rays for manganese substituted nano hydroxyapatite. *Radiation Physics and Chemistry*, 159, 76-80. https://doi.org/10.1016/j.radphyschem.2019.02.040

Kokubo, T., & Takadama, H. (2006). How useful is SBF in predicting in vivo bone bioactivity? *Biomaterials*, *27*(15), 2907–2915. https://doi.org/10.1016/J.BIOMATERIALS.2006.01.017

Landi, E., Celotti, G., Logroscino, G., & Tampieri, A. (2003). Carbonated hydroxyapatite as bone substitute. *Journal of the European Ceramic Society*, *23*(15), 2931–2937. https://doi.org/10.1016/S0955-2219(03)00304-2

Lanza, R., Langer, R., Vacanti, J. P., & Atala, A. (2020). *Principles of Tissue Engineering*. Academic Press, Elsevier, 5th Edition. https://doi.org/10.1016/B978-0-12-818422-6.00004-6

Lee, J. M., Choi, B. B. R., Choi, J. H., Kim, G. C., Hwang, D. S., Chang, M. C., Byun, J. H., & Kim, U. K. (2013). Osteoblastic response to the hydroxyapatite/gelatin nanocomposite and bio-calcium phosphate cement. *Tissue Engineering and Regenerative Medicine*, *10*(2), 47–52. https://doi.org/10.1007/S13770-013-0344-1/METRICS

Li, Y., Yu, Z., Ai, F., Wu, C., Zhou, K., Cao, C., & Li, W. (2021). Characterization and evaluation of polycaprolactone/hydroxyapatite composite scaffolds with extra surface morphology by cryogenic printing for bone tissue engineering. *Materials & Design*, *205*, 109712. https://doi.org/10.1016/j.matdes.2021.109712

Lien, S. M., Ko, L. Y., & Huang, T. J. (2009). Effect of pore size on ECM secretion and cell growth in gelatin scaffold for articular cartilage tissue engineering. *Acta Biomaterialia*, *5*(2), 670–679. https://doi.org/10.1016/J.ACTBIO.2008.09.020

Lien, S. M., Li, W. te, & Huang, T. J. (2008). Genipin-crosslinked gelatin scaffolds for articular cartilage tissue engineering with a novel crosslinking method. *Materials Science and Engineering: C*, *28*(1), 36–43. https://doi.org/10.1016/J.MSEC.2006.12.015

Long, T., Yang, J., Shi, S. S., Guo, Y. P., Ke, Q. F., & Zhu, Z. A. (2015). Fabrication of three-dimensional porous scaffold based on collagen fiber and bioglass for bone tissue engineering. *Journal of Biomedical Materials*

Research. Part B, Applied Biomaterials, *103*(7), 1455–1464. https://doi.org/10.1002/JBM.B.33328

Lozzi, I., Pucci, A., Pantani, O. L., D'Acqui, L. P., & Calamai, L. (2008). Interferences of suspended clay fraction in protein quantitation by several determination methods. *Analytical biochemistry*, *376*(1), 108-114. https://doi.org/10.1016/j.ab.2008.01.040

Lu, T., Li, Y., & Chen, T. (2013). Techniques for fabrication and construction of three-dimensional scaffolds for tissue engineering. *International Journal of Nanomedicine, 8*, 337–350. https://doi.org/10.2147/IJN.S38635

Lysaght, M. J., & Reyes, J. (2001). The growth of tissue engineering, *Tissue Engineering*, *7*(5), 485–493. https://doi.org/10.1089/107632701753213110

Mallick, M., Are, R. P., & Babu, A. R. (2022). An overview of collagen/bioceramic and synthetic collagen for bone tissue engineering. *Materialia*, *22*, 101391. https://doi.org/10.1016/J.MTLA.2022.101391

Mayer, I., Cuisinier, F. J. G., Popov, I., Schleich, Y., Gdalya, S., Burghaus, O., & Reinen, D. (2006). Phase elations between β-tricalcium phosphate and hydroxyapatite with manganese(II): Structural and spectroscopic properties. *European Journal of Inorganic Chemistry*, *2006*(7), 1460–1465. https://doi.org/10.1002/EJIC.200501009

Mayer, I., Diab, H., Reinen, D., & Albrecht, C. (1993). Manganese in apatites, chemical, ligand-field and electron paramagnetic resonance spectroscopy studies. *Journal of Materials Science, 28*, 2428-2432. https://doi.org/10.1007/BF01151675

Meireles, A. B., Corrêa, D. K., da Silveira, J. V. W., Millás, A. L. G., Bittencourt, E., de Brito-Melo, G. E. A., & González-Torres, L. A. (2018). Trends in polymeric electrospun fibers and their use as oral biomaterials. *Experimental Biology and Medicine, 243*(8), 665–676. https://doi.org/10.1177/1535370218770404

Mohamed, A. M. (2008). An overview of bone cells and their regulating factors of differentiation. *The Malaysian Journal of Medical Sciences, 15*(1), 4-12. PMCID: PMC3341892.

Molnar, C., & Gair, J. (2015). *Concepts of Biology – 1st Canadian Edition*, Chapter 19.2: Bone, BCcampus.

Moreira, M. P., de Almeida Soares, G. D., Dentzer, J., Anselme, K., de Sena, L. Á., Kuznetsov, A., & dos Santos, E. A. (2016). Synthesis of magnesium- and manganese-doped hydroxyapatite structures assisted by the simultaneous incorporation of strontium. *Materials Science and Engineering: C*, *61*, 736–743. https://doi.org/10.1016/J.MSEC.2016.01.004

Morgan, E. F., & Gerstenfeld, L. C. (2021). The bone organ system: form and function. In *Marcus and Feldman's Osteoporosis* (pp. 15-35). Academic Press. https://doi.org/10.1016/B978-0-12-813073-5.00002-2

Muschler, G. F., Nakamoto, C., & Griffith, L. G. (2004). Engineering principles of clinical cell-based tissue engineering. *The Journal of Bone and Joint Surgery*, *86*(7), 1541-1558. https://doi.org/10.2106/00004623-200407000-00029

Nahian, A., & Chauhan, P. R. (2022). Histology, Periosteum and Endosteum. *StatPearls Publishing*. https://www.ncbi.nlm.nih.gov/books/NBK557584/

Natasha, A. N., Sopyan, I., & Zuraida, A. (2008). Fourier transform infrared study on sol-gel derived manganese-doped hydroxyapatite. *Advanced Materials Research*, *47–50*, 1185–1188. https://doi.org/10.4028/WWW.SCIENTIFIC.NET/AMR.47-50.1185

Nemani, S. K., Annavarapu, R. K., Mohammadian, B., Raiyan, A., Heil, J., Haque, M. A., Abdelaal, A., & Sojoudi, H. (2018). Surface modification of polymers: methods and applications. *Advanced Materials Interfaces*, *5*(24), 1801247. https://doi.org/10.1002/admi.201801247

Nicolais, L., Gloria, A., & Ambrosio, L. (2010). The mechanics of biocomposites. *Biomedical Composites*, Woodhead Publishing, 411–440. https://doi.org/10.1533/9781845697372.3.411

Paluszkiewicz, C., Ślósarczyk, A., Pijocha, D., Sitarz, M., Bućko, M., Zima, A., Chróścicka, A., & Lewandowska-Szumieł, M. (2010). Synthesis, structural properties and thermal stability of Mn-doped hydroxyapatite. *Journal of Molecular Structure*, *976*(1–3), 301–309. https://doi.org/10.1016/J.MOLSTRUC.2010.04.001

Park, S. A., Lee, S. H., & Kim, W. D. (2011). Fabrication of porous polycaprolactone/hydroxyapatite (PCL/HA) blend scaffolds using a 3D plotting system for bone tissue engineering. *Bioprocess and biosystems engineering*, *34*, 505-513. https://doi.org/10.1007/s00449-010-0499-2

Pattanashetti, N. A., Viana, T., Alves, N., Mitchell, G. R., & Kariduraganavar, M. Y. (2020). Development of novel 3D scaffolds using BioExtruder by varying the content of hydroxyapatite and silica in PCL matrix for bone tissue engineering. *Journal of Polymer Research*, *27*(4), 1–13. https://doi.org/10.1007/S10965-020-02053-0/FIGURES/10

Paz, A., Guadarrama, D., López, M., González, J. E., Brizuela, N., & Aragón, J. (2012). A comparative study of hydroxyapatite nanoparticles synthesized by different routes. *Química Nova*, *35*(9), 1724–1727. https://doi.org/10.1590/S0100-40422012000900004

Petre, D. G., & Leeuwenburgh, S. C. G. (2022). The use of fibers in bone tissue engineering. *Tissue Engineering: Part B*, *28*(1), 141–159. https://doi.org/10.1089/TEN.TEB.2020.0252

Poovendran, K., Josephwilson, K. S., Sakthipandi, K., & Ramanujam, N. R. (2022). Assimilation of manganese metal ion doped hydroxyapatite by Co-Precipitation technique. *Journal of the Indian Chemical Society*, *99*(11), 100779. https://doi.org/10.1016/j.jics.2022.100779

Qin, X., Wu, Y., Liu, S., Yang, L., Yuan, H., Cai, S., ... & Yu, C. (2022). Surface modification of polycaprolactone scaffold with improved biocompatibility and controlled growth factor release for enhanced stem cell differentiation. *Frontiers in Bioengineering and Biotechnology*, *9*, 802311. https://doi.org/10.3389/fbioe.2021.802311

Ramesh, S., Tan, C. Y., Peralta, C. L., & Teng, W. D. (2007). The effect of manganese oxide on the sinterability of hydroxyapatite. *Science and Technology of Advanced Materials*, *8*(4), 257-263. https://doi.org/10.1016/j.stam.2007.02.006

Ratner, B. D. (1995). Surface modification of polymers: chemical, biological and surface analytical challenges. *Biosensors and bioelectronics*, *10*(9-10), 797-804. https://doi.org/10.1016/0956-5663(95)99218-A

Ratner, B. D., Hoffman, A. S., Schoen, F. J., & Lemons, J. E. (2013). Introduction - Biomaterials Science: An Evolving, Multidisciplinary Endeavor. *Biomaterials Science: An Introduction to Materials: Third Edition*, xxv–xxxix. https://doi.org/10.1016/B978-0-08-087780-8.00153-4

Raynaud, S., Champion, E., Bernache-Assollant, D., & Thomas, P. (2002). Calcium phosphate apatites with variable Ca/P atomic ratio I. Synthesis, characterisation and thermal stability of powders. *Biomaterials*, *23*(4), 1065–1072. https://doi.org/10.1016/S0142-9612(01)00218-6

Reid, J. W., Tuck, L., Sayer, M., Fargo, K., & Hendry, J. A. (2006). Synthesis and characterization of single-phase silicon-substituted α-tricalcium phosphate. *Biomaterials*, *27*(15), 2916–2925. https://doi.org/10.1016/J.BIOMATERIALS.2006.01.007

Safadi, F. F., Barbe, M. F., Abdelmagid, S. M., Rico, M. C., Aswad, R. A., Litvin, J., & Popoff, S. N. (2009). Bone structure, development and bone biology. *Bone Pathology*, 1–50. https://doi.org/10.1007/978-1-59745-347-9_1

Sarasua, J. R., López-Rodríguez, N., Zuza, E., Petisco, S., Castro, B., Del Olmo, M., ... & Alonso-Varona, A. (2011). Crystallinity assessment and in vitro cytotoxicity of polylactide scaffolds for biomedical applications. *Journal of Materials Science: Materials in Medicine*, *22*, 2513-2523.

Sharma, N., & Sharma, S. (2021). Anticorrosive coating of polymer composites: A review. *Materials Today: Proceedings*, *44*, 4498-4502. https://doi.org/10.1016/j.matpr.2020.10.726

Shor, L., Güçeri, S., Wen, X., Gandhi, M., & Sun, W. (2007). Fabrication of three-dimensional polycaprolactone/hydroxyapatite tissue scaffolds and osteoblast-scaffold interactions in vitro. *Biomaterials*, *28*(35), 5291-5297. https://doi.org/10.1016/j.biomaterials.2007.08.018

Sopyan, I., Ramesh, S., Nawawi, N. A., Tampieri, A., & Sprio, S. (2011). Effects of manganese doping on properties of sol–gel derived biphasic calcium phosphate ceramics. *Ceramics International*, *37*(8), 3703-3715. https://doi.org/10.1016/j.ceramint.2011.06.033

Tian, G., Zhu, G., Xu, S., & Ren, T. (2019). A novel shape memory poly (ε-caprolactone)/hydroxyapatite nanoparticle networks for potential biomedical applications. *Journal of Solid State Chemistry*, *272*, 78-86. https://doi.org/10.1016/j.jssc.2019.01.029

Truesdell, S. L., & Saunders, M. M. (2020). Bone remodeling platforms: Understanding the need for multicellular lab-on-a-chip systems and predictive agent-based models. *Mathematical Biosciences and Engineering*, *17*(2), 1233–1252. https://doi.org/10.3934/MBE.2020063

Wallace, J. M., Orr, B. G., Marini, J. C., & Holl, M. M. B. (2011). Nanoscale morphology of Type I collagen is altered in the Brtl mouse model of Osteogenesis Imperfecta. *Journal of Structural Biology*, *173*(1), 146–152. https://doi.org/10.1016/J.JSB.2010.08.003

Wang, Y., Liu, L., & Guo, S. (2010). Characterization of biodegradable and cytocompatible nano-hydroxyapatite/polycaprolactone porous scaffolds in degradation in vitro. *Polymer Degradation and Stability*, *95*(2), 207-213. https://doi.org/10.1016/j.polymdegradstab.2009.11.023

Williams, D. F., (1987). Definitions in Biomaterials. Proceedings of a Consensus Conference of the European Society for Biomaterials, Chester, England, March 3–5 1986, Vol. 4, Elsevier, New York.

Wu, X., Walsh, K., Hoff, B. L., & Camci-Unal, G. (2020). Mineralization of biomaterials for bone tissue engineering. *Bioengineering*, *7*(4), 1–24. https://doi.org/10.3390/BIOENGINEERING7040132

Xidaki, D., Agrafioti, P., Diomatari, D., Kaminari, A., Tsalavoutas-Psarras, E., Alexiou, P., Psycharis, V., Tsilibary, E. C., Silvestros, S., & Sagnou, M. (2018). Synthesis of hydroxyapatite, β-Tricalcium phosphate and biphasic calcium phosphate particles to act as local delivery carriers of curcumin: Loading, release and in vitro studies. *Materials*, *11*(4), 595. https://doi.org/10.3390/MA11040595

Yedekçi, B., Tezcaner, A., Yılmaz, B., Demir, T., & Evis, Z. (2022). 3D porous PCL-PEG-PCL / strontium, magnesium and boron multi-doped hydroxyapatite composite scaffolds for bone tissue engineering. *Journal of the Mechanical Behavior of Biomedical Materials*, *125*, 104941. https://doi.org/10.1016/J.JMBBM.2021.104941

Zhang, S., Prabhakaran, M. P., Qin, X., & Ramakrishna, S. (2015). Biocomposite scaffolds for bone regeneration: Role of chitosan and hydroxyapatite within poly-3-hydroxybutyrate-co-3-hydroxyvalerate on mechanical properties and in vitro evaluation. *Journal of the Mechanical Behavior of Biomedical Materials*, *51*, 88–98. https://doi.org/10.1016/J.JMBBM.2015.06.032